



Available online at www.sciencedirect.com



Journal of Computational Physics 207 (2005) 192–220

JOURNAL OF
COMPUTATIONAL
PHYSICS

www.elsevier.com/locate/jcp

Calibrated reduced-order POD-Galerkin system for fluid flow modelling

M. Couplet ^{a,*}, C. Basdevant ^b, P. Sagaut ^c

^a ONERA, Computational Fluid Dynamics and Aeroacoustics Department, 29 av. de la Division Leclerc, BP 72, 92322 Châtillon, France

^b LMD, École Normale Supérieure, 24 rue Lhomond, 75231 Paris Cedex 5, France

^c LMM, Université Pierre et Marie Curie, Boîte 162, 4 place Jussieu, 75252 Paris Cedex 5, France

Received 14 June 2004; received in revised form 19 November 2004; accepted 12 January 2005

Available online 22 February 2005

Abstract

To improve the behaviour of reduced-order proper orthogonal decomposition (POD)-Galerkin systems, two numerical methods are proposed. These methods determine free parameters in the POD-Galerkin system from flow simulations via a minimization problem. They give rise to linear systems and their computational costs are reasonable. Both methods are assessed for two flow configurations: a two-dimensional flow around a square-cylinder for a Reynolds number of 100 and a three-dimensional flow past a backward-facing step for a Reynolds number of 7432 based on the step height and the streamwise velocity at the middle of the inlet. For both configurations, the methods are effective since accurate calibrated reduced-order POD-Galerkin systems are obtained.

© 2005 Elsevier Inc. All rights reserved.

Keywords: Reduced-order flow modelling; POD-Galerkin method; Optimization

1. Introduction

The proper orthogonal decomposition (POD, also known as Karhunen–Loève decomposition and principal component analysis) is a theoretical and post-processing tool to reduce global coherent structures of flows thus to describe and analyze them. Moreover, since laminar and transitional fluid flows are very often governed by a small number of coherent structures, it is interesting to use the spatial POD functions, called POD modes, as basis functions for a Galerkin method in order to construct a system of ordinary differential

* Corresponding author.

E-mail addresses: couplet@onera.fr, mathieu.couplet@laposte.net (M. Couplet), basdevant@lmd.ens.fr (C. Basdevant), sagaut@lmm.jussieu.fr (P. Sagaut).

equations (ODEs) which approximates the whole flow dynamics. Therefore, after truncating the POD modal basis by keeping only the main POD modes, a ODE system of small dimension can be extracted from numerical data (see [1] for a survey): this system is called (reduced-order) POD-Galerkin system.

As an effective technique of low-order modelling, the POD-Galerkin method is attractive for flow control (see [2–4]). However, especially for transitional and turbulent flows, the low-order ODE systems obtained may be barely accurate and even sometimes unstable.

A first reason is the intrinsic gap that may exist between the nature of the data whose POD is performed and the variational formulation on which the Galerkin method is based. For instance, experimental data of a flow at low Mach number may not satisfy very accurately the variational formulation derived from the incompressible Navier–Stokes equations, or data provided by finite-volume codes are not computed via the numerical discretization of a variational formulation. This can bring about a lack of effectiveness of the POD-Galerkin method in practice in numerous cases.

A second and main reason is that the low-order truncation of the POD basis inhibits generally all the transfers between the large and the small (unresolved) scales of the fluid flow. In consequence, to recover the effects of the truncated modes, that is generally of the small scales, two different ways have been studied in the literature: the definition of POD in the H^1 Sobolev space rather than in L^2 [5], or the use of “eddy” viscosities [6,7]. That use of artificial viscosities, whose relevance was investigated for a separated non-homogeneous turbulent flow in [8], amounts to perturbing the viscous terms of the POD-Galerkin system. As mentioned by Sirisup et al. [9], the add of artificial viscosities remains interesting for two-dimensional flows with Reynolds numbers of the order of 100 for correcting the long-term behaviour of POD-Galerkin systems. Furthermore, if the boundary conditions are disregarded when the Galerkin method is applied (it can be indeed difficult to deal with complex unsteady Dirichlet conditions in practice, see Appendix A for explanations), the modelling of the pressure term may pose problems. Moreover, the computation of a POD-Galerkin system is subject to numerical errors, which may be very prejudicial since such an ODE system can be very sensitive. So it appears interesting to develop methods to increase the accuracy of reduced-order POD-Galerkin models and to improve the modelling skills of the POD-Galerkin method.

To correct the behaviour of a low-order POD-Galerkin system, two numerical methods are here proposed and assessed. They consist in adjusting the polynomial coefficients which define the POD-Galerkin system by solving a minimization problem: the new ODE system has to recover optimally the dynamics of the data used to construct the POD and is computed in taking the original POD-Galerkin system into account.

A similar principle was investigated by Galletti et al. [10] to calculate some linear models of terms relevant to the pressure in the construction of a POD-Galerkin system of laminar flow regimes past a square cylinder. Here, we propose to modify all the coefficients (linear and quadratic) of the POD-Galerkin system to improve it. Moreover, the methods are assessed on a turbulent flow configuration where the main challenge is the modelling of the effect of the truncated POD modes (that is the small scales). Furthermore, it is worthy of note that the cost functions used in the present paper are designed to control the way the initial POD-Galerkin system is modified (thanks to the cost function \mathcal{D} , see Section 3.1), which is very interesting in practice (refer to the observations of Sections 4.2 and 4.3).

The computational costs of these methods are reasonable since they use the temporal part of the POD information, whereas the Galerkin method uses the spatial POD information (that is the POD modes themselves), much more voluminous in practice, to construct the ODE system (see Section 3.4 for further details). This motivates the development of calibration methods: a clever use of the spatial POD information could enable large computational saving for reduced-order system from very demanding computations.

The reduced-order POD-Galerkin fluid flow modelling is described and applied to two configurations in Section 2: to a two-dimensional quasi-incompressible laminar flow around a square–cylinder and to a three-dimensional incompressible turbulent flow past a backward-facing step. The general principle of the

calibration of low-order POD-Galerkin systems is formally presented then the numerical methods are proposed in Section 3. These calibration methods are finally assessed in Section 4 for both flow configurations.

2. The reduced-order POD-Galerkin modelling

In this section, the POD-Galerkin method is described for the modelling of an incompressible flow (details about treatment of the boundary conditions are displayed in [Appendix A](#)). Then few results for the two test flow configurations which were used in our numerical experiments are presented.

2.1. POD-Galerkin method for incompressible flows

The POD is applied to a velocity field $\mathbf{u}^e \in \mathbb{R}^d$ which is known over the time interval $[0, T]$ and the physical space $\Omega \subset \mathbb{R}^d$ ($d = 2$ or 3). That is $\mathbf{u}^e \in L^2(0, T, L^2(\Omega)^d)$ is decomposed into an orthonormal basis of spatial functions φ_i of $L^2(\Omega)^d$, called POD modes, for each time $t \in [0, T]$:

$$\mathbf{u}^e(\mathbf{x}, t) = \sum_i \underbrace{(\mathbf{u}^e, \varphi_i)}_{a_i^e(t)} \varphi_i(\mathbf{x}) \quad \forall (\mathbf{x}, t) \in \Omega \times [0, T], \quad (1)$$

where (\cdot, \cdot) is the classical $L^2(\Omega)^d$ inner product on the flow domain and where the $a_i^e(t)$ are the time-dependent coefficients of the decomposition. For an incompressible flow (with a unitary constant density), the mean kinetic energy per mass unit captured by the i th POD mode φ_i is

$$\frac{1}{T} \int_0^T a_i^e(t)^2 dt = \lambda_i \quad (2)$$

and the basis is ordered such that $\lambda_i \geq \lambda_{i+1}$ for all i . In all the following, σ_i will denote $\sqrt{\lambda_i}$. The POD basis is constructed to be optimal in the sense that, for any M and any orthonormal tuple (ψ_1, \dots, ψ_M) of $L^2(\Omega)^{dM}$,

$$\frac{1}{T} \int_0^T \left\| \mathbf{u}^e - \sum_{i=1}^M (\mathbf{u}^e, \varphi_i) \varphi_i \right\|_{L^2}^2 dt \leq \frac{1}{T} \int_0^T \left\| \mathbf{u}^e - \sum_{i=1}^M (\mathbf{u}^e, \psi_i) \psi_i \right\|_{L^2}^2 dt. \quad (3)$$

From a physical point of view, the first M modes, φ_i for $i \in \{1, \dots, M\}$, capture more kinetic energy of \mathbf{u}^e on average over $[0, T]$ than any other set of M orthonormal spatial functions. Since the kinetic energy captured by the first M modes is $\sum_{i=1}^M \lambda_i$, the decrease of the POD spectrum, that is of the distribution of the λ_i with respect to the index i , quantifies the efficiency of the POD.

This optimality property of the POD explains why the first M POD modes, for M large enough, are interesting candidates for a Galerkin method. The POD-Galerkin system obtained is labeled as reduced-order since the POD basis is truncated by neglecting the POD modes φ_i for $i > M$.

The POD-Galerkin system is constructed by applying the Galerkin method, using the space spanned by the first M POD modes. The variational formulation is generally deduced from the velocity-pressure expressions of the non-dimensional Navier–Stokes equations, considering a solenoidal test function φ (indeed, the POD modes keep some properties of \mathbf{u}^e as vanishing divergence):

$$\frac{d}{dt}(\mathbf{u}, \varphi) + ((\mathbf{u} \cdot \nabla) \mathbf{u}, \varphi) + \frac{1}{Re} \sum_{i=1}^d (\nabla u_{x_i}, \nabla \varphi_{x_i}) + T_{\partial\Omega} = (\mathbf{h}, \varphi), \quad (4)$$

where \mathbf{u} is the velocity field, Re is the Reynolds number, \mathbf{h} is a source term (force field independent of the flow), $u_{x_i} = \mathbf{u} \cdot \mathbf{x}_i$ and $\varphi_{x_i} = \varphi \cdot \mathbf{x}_i$ are the component of \mathbf{u} and φ in the spatial direction of the unitary vector

\mathbf{x}_i ($1 \leq i \leq d$) and where $T_{\partial\Omega}$ is a boundary term (consult Appendix A for further details about it and the explicit treatment of the boundary conditions).

Therefore, under the assumption that the reduced POD basis is suitable (that is the M first modes are sufficient to accurately represent the flow), a M -dimensional polynomial ODE system is derived by taking the M first POD modes as basis and test functions. More precisely, if $\mathbf{h} = 0$ and $T_{\partial\Omega} = 0$, the POD-Galerkin system is

$$\dot{\mathbf{a}}^g(t) = f^g(\mathbf{a}^g(t)) = \begin{bmatrix} f_1^g(a^g(t)) \\ \vdots \\ f_M^g(a^g(t)) \end{bmatrix}, \quad \text{where } \mathbf{a}^g(t) = \begin{bmatrix} a_1^g(t) \\ \vdots \\ a_M^g(t) \end{bmatrix} \in \mathbb{R}^M, \quad (5)$$

and each polynomial f_i^g can be expressed as

$$f_i^g(\mathbf{a}^g) = \sum_{k=1}^M \frac{C_i^k}{Re} a_k^g + \sum_{k=1}^M \sum_{j=1}^M C_i^{k,j} a_k^g a_j^g, \quad (6)$$

with

$$C_i^k = - \sum_{j=1}^d \left(\nabla(\varphi_k)_{x_j}, \nabla(\varphi_i)_{x_j} \right) \quad \text{and} \quad C_i^{k,j} = - \left((\varphi_k \cdot \nabla) \varphi_j, \varphi_i \right). \quad (7)$$

Furthermore, when non-homogeneous Dirichlet boundary conditions for the velocity are considered, the POD is generally applied to $\mathbf{u}^e(\mathbf{x}, t) - \bar{\mathbf{u}}^e(\mathbf{x}, t)$ instead of \mathbf{u}^e , with $\bar{\mathbf{u}}^e$ chosen so that $\mathbf{u}^e - \bar{\mathbf{u}}^e$ satisfies homogeneous Dirichlet boundary conditions (see Appendix A). In that case, the contribution of $\bar{\mathbf{u}}^e$ has to be added to system (5) together with the contributions of $T_{\partial\Omega}$ and \mathbf{h} . In the flow configurations of Sections 2.2 and 2.3, the Dirichlet conditions for the velocity are non-homogeneous yet unsteady and $\bar{\mathbf{u}}^e$ is simply chosen as the mean velocity field: the POD computed corresponds to the fluctuant velocity. In fact, in the case of the turbulent configuration (Section 2.3), the inlet Dirichlet boundary condition is not strictly unsteady however it is realistic to perform the POD on the fluctuant velocity and to neglect the boundary term since the fluctuant velocity and its POD modes take very small values at the inlet (see [8]).

Finally, the general form of the POD-Galerkin system obtained is

$$\dot{\mathbf{a}}^g(t) = f^g(\mathbf{a}^g(t)) + r(t) \quad \text{and} \quad \mathbf{a}^g(0) = \mathbf{a}^e(0), \quad (8)$$

where $\mathbf{a}^e(0)$ are the initial conditions, f^g is a vector polynomial of degree 2 in the components of \mathbf{a}^g and r takes the contributions of the source term \mathbf{h} , of the boundary term $T_{\partial\Omega}$ and of $\bar{\mathbf{u}}^e$ into account.

In the following, the methods are presented for $r = 0$ for the sake of clarity. Moreover, in the modelling of the two test flow configurations used here, $\bar{\mathbf{u}}^e$ is unsteady, $\mathbf{h} = 0$ and the boundary term $T_{\partial\Omega}$ vanishes (refer to Appendix A), thus r is independent of the time: the constant vector r is simply considered as a term of degree zero of f^g in the numerical experiments of Section 4.

Notice that a polynomial POD-Galerkin system can also be constructed in the compressible case for a perfect gas by performing the POD on the suitable set of flow variables (the inverse of the density ρ^{-1} , the velocity \mathbf{u} and the pressure p): see [11] or [5]. In consequence, the methods proposed here can be theoretically applied to compressible cases without any modifications although the numerical experiments presented here were only performed for the incompressible configurations of Sections 2.2 and 2.3.

In conclusion, given numerical data for the flow field \mathbf{u}^e , that is, for example, given a set of N snapshots along a time interval $[0, T]$, a POD basis $(\varphi_i)_{1 \leq i \leq N}$ can be obtained such that $\mathbf{u}^e(t) = \bar{\mathbf{u}}^e(t) + \sum_{1 \leq i \leq N} a_i^e(t) \varphi_i$. The POD-Galerkin system is then formed by evaluating a variational formulation of the governing equations with the M first POD modes. The questions are then: is the solution $\mathbf{a}^g(t)$ to (8) a good approximation of the true time coefficients $a^e(t)$? And, if not, how to modify (8) to improve the model?

2.2. Two-dimensional flow with a Reynolds number of 100

The first test configuration is a quasi-incompressible two-dimensional vortex-shedding flow around a square cylinder for $Re = 100$. The database was computed by a compressible finite-volume code for a Mach number of 10^{-3} (see [12] for details) and is composed of $N = 480$ snapshots of the velocity over one shedding cycle of the Von Kármán vortex street (that is for $[0, T]$). Some vorticity contours of the fluctuant velocity at time $t = T/2$ are plotted in Fig. 1.

From the POD of the fluctuant velocity performed by the snapshot method (see [13]), a 6-mode POD-Galerkin system was computed. The first six POD modes capture more than 99.9% of the fluctuant kinetic energy of the database $K_N = \sum_{i=1}^N \lambda_i$:

i	1	2	3	4	5	6
λ_i/K_N	0.486	0.482	1.214×10^{-2}	1.209×10^{-2}	3.756×10^{-3}	3.744×10^{-3}

The spectrum is plotted in logarithmic scale for the first 16 modes in Fig. 2. Iso-lines of the transverse components of the first six modes are plotted in Fig. 3. These figures show that the first POD modes can be naturally grouped by pairs. This is coherent with the nature of the vortex shedding flow and with many preceding works, for instance [14]. Moreover, the flow topology is consistent with the results of the latter paper.

Values of $f_1^g(a^e(t))$ and $f_2^g(a^e(t))$ are compared to $\dot{a}_1^e(t)$ and $\dot{a}_2^e(t)$ in Fig. 4. The histories of $a_1^g(t)$ and $a_2^g(t)$ computed from the 6-mode system are displayed on the same figure with $a_1^e(t)$ and $a_2^e(t)$ (all the simulations of the polynomial POD-Galerkin systems were performed with a classical fourth-order Runge–Kutta scheme).

The 6-mode system gives a good approximation of the dynamics of the two first POD modes, however its simulation shows that the system is not able to reproduce very accurately the history of a^e since there is a noticeable difference between a_1^e and a_2^e at $t = T$. This gap has three causes: the numerical errors, the effects of the truncation of the POD basis and the fact that the data do not perfectly fit the variational formulation (4) by nature.

2.3. Three-dimensional turbulent flow

The second test configuration is a three-dimensional incompressible turbulent flow past a backward facing step. The database was provided by an incompressible finite-difference large-Eddy simulation (see [15]) and is formed of $N = 1000$ snapshots of the velocity for a time interval $[0, T]$ long enough to encompass at least one period of the low-frequency breathing mode of the recirculation bubble: $T = 37.5h/U = 50h/\bar{U}$ where h is the step height, U the streamwise velocity at the middle of the inlet and \bar{U} the mean streamwise

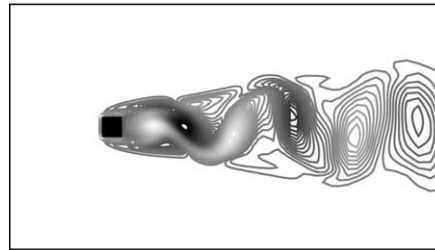


Fig. 1. Iso-lines of the vorticity of the fluctuant velocity at time $t = T/2$ on half the computational domain in the streamwise direction.

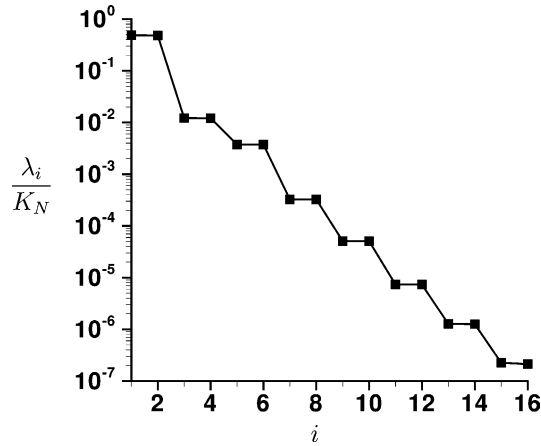


Fig. 2. The 16 first values of the POD spectrum of the square cylinder flow in logarithmic scale.

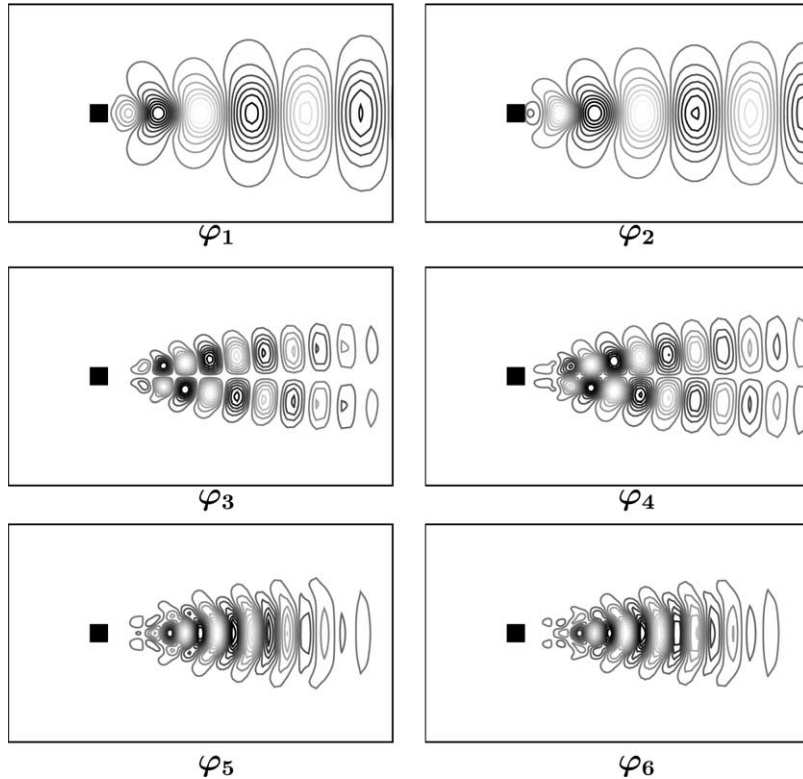


Fig. 3. Iso-lines of the transverse components of φ_1 , φ_2 , φ_3 , φ_4 , φ_5 and φ_6 on half the computational domain in the streamwise direction.

velocity at the entrance. The Reynolds number based on U and h is 7432 and the one based on \bar{U} and the height $10h$ of the channel above the step is 66,000. The geometry of the computational domain is presented in Fig. 5.

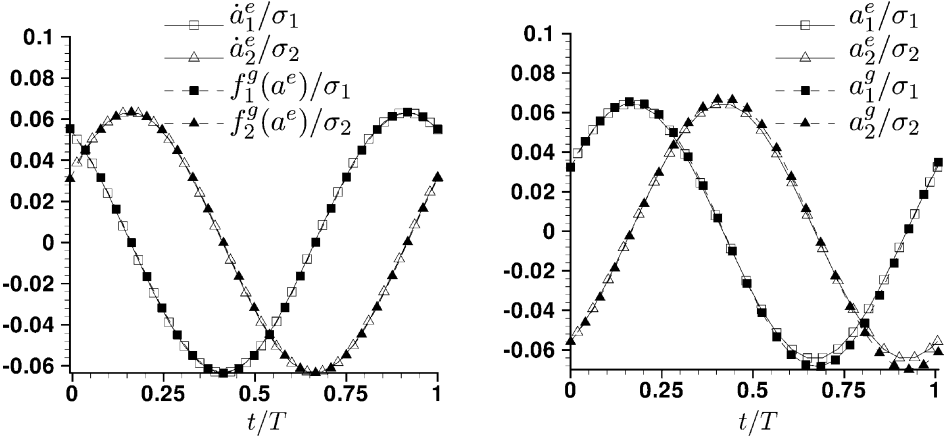


Fig. 4. Comparison of the dynamics (left) and of the history (right) of the data with the behaviour of 6-mode POD-Galerkin system for the two first modes.

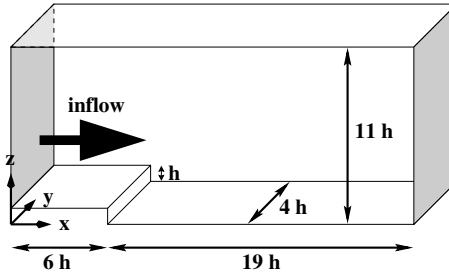


Fig. 5. Geometry of the computational domain which corresponds to the spatial extent of the POD modes.

The POD of the fluctuant velocity was performed by the snapshot method using the full database. Fig. 6 shows some Q-isosurfaces of the mean velocity \bar{u}^e and of the POD modes φ_1 , φ_{20} and φ_{40} . The POD spectrum is presented in logarithmic scale in Fig. 7: the POD is quite efficient according to the decrease of the spectrum.

Notice that the POD of such a step flow is presented in [16] for a Reynolds number about twice smaller and that a low compactness of the kinetic energy distribution within the POD basis is observed. Three facts make it possible to understand this difference. Firstly, the database of [16] was computed by direct numerical simulation so contains a larger range of structures than our LES database. Secondly, the POD is combined with a Fourier decomposition which is not strictly equivalent to a full POD (which is optimal) even if a spectrum close to the POD spectrum is generally expected. Thirdly, the time interval over which the flow is analyzed is twelve times longer in [16], considering some time units based on the step height and on the maximum inlet streamwise velocity in a transverse plane located before the step (0.07h and 6h from the step in [16] and in our case, respectively).

The POD-Galerkin polynomial f^g computed takes the first $M = 86$ modes which capture more than 99.9% of the fluctuant kinetic energy into account. That POD-Galerkin system was defined as explained in Section 2.1 and in Appendix A: the system is based on the classical Navier–Stokes equations, not on the filtered Navier–Stokes equations and the subgrid model used to perform the LES of the flow.

Taking the subgrid model into consideration might be a benefit, however disregarding it considerably simplifies the reduced-order modelling; furthermore and above all, we would like to point out that neglect-

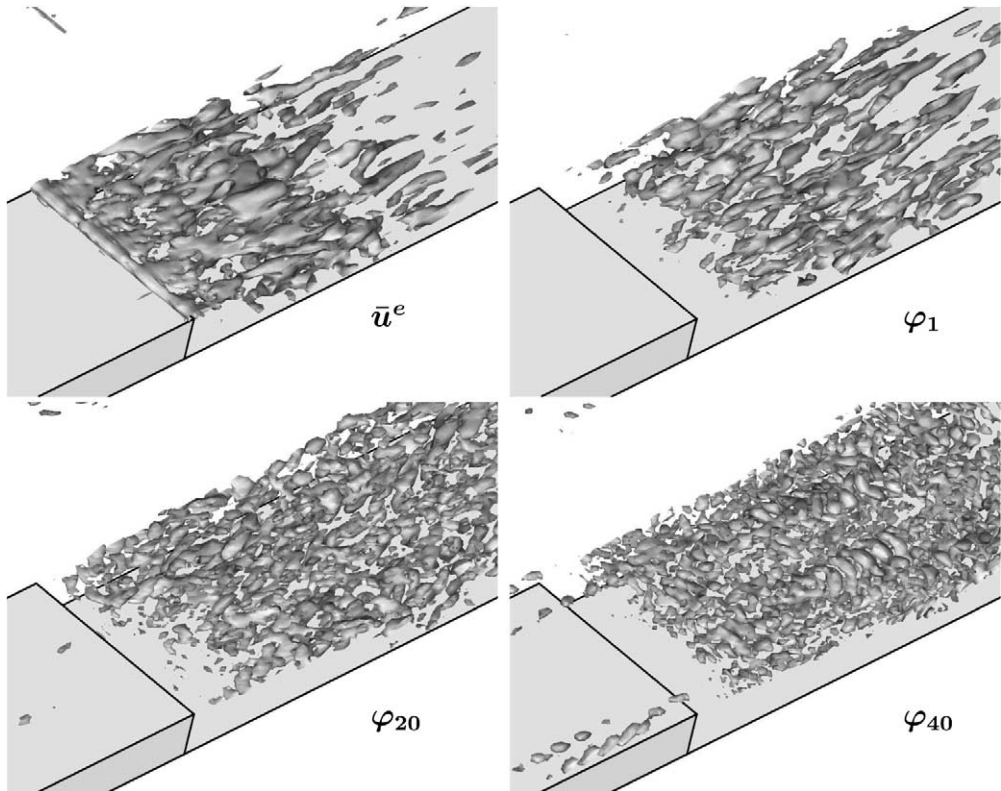


Fig. 6. Visualization of the main structures of \bar{u}^e , φ_1 , φ_{20} and φ_{40} (Q-isosurface).

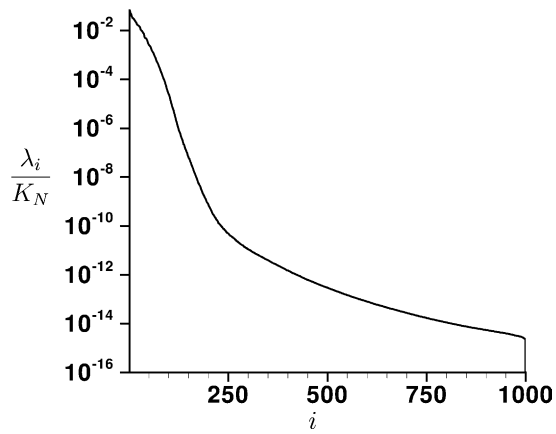


Fig. 7. Logarithmic POD spectrum of the step flow.

ing the last POD modes, which is the basis of the reduced-order POD-Galerkin modelling, has by nature a stronger impact than neglecting the subgrid model: the structures of the neglected POD modes are necessarily larger than the unresolved scales and play in consequence a more important role in the flow dynamics.

That is why the approach chosen here consists in a way in including the modelling of the subgrid scales in the modelling of the neglected POD modes, this will be performed by a calibration of the ODE system.

Fig. 8 compares the behaviours of the data and of the 86-mode POD-Galerkin system for the first and fifth modes. The lack of accuracy of the reduced-order system is obvious for this turbulent three-dimensional configuration. Indeed, a^g diverges from a^e and it seems that the system does not dissipate enough energy.

3. Definition of the methods

In the following, the calibration methods designed to improve the POD-Galerkin system are presented for $r = 0$ for the sake of clarity.

3.1. The general formulation

The polynomial f^α , which determines the calibrated system we are looking for, will be defined as the solution to an optimization problem. f^α should minimize a functional \mathcal{J}^α :

$$\mathcal{J}^\alpha(f) = (1 - \alpha)\mathcal{E}(f) + \alpha\mathcal{D}(f), \quad (9)$$

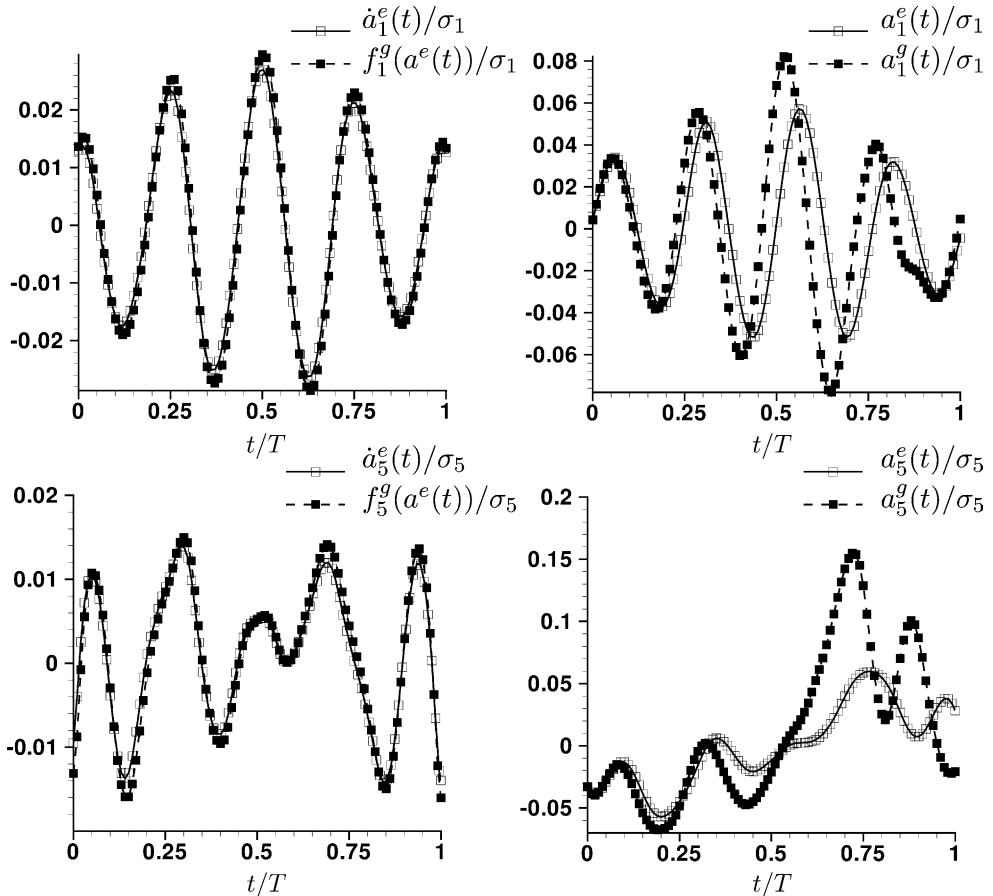


Fig. 8. Comparison of the dynamics (left) and of the history (right) of the data with the behaviour of the POD-Galerkin model of the step flow for the 1st (top) and 5th (bottom) modes.

where $\alpha \in [0,1]$ is a weighing parameter, $\mathcal{E}(f)$ measures the “error” between the behaviour of the data, that is the one of $a^e(t)$, and the behaviour of the dynamical system associated to f whose state is $a(t)$ and where $\mathcal{D}(f)$ is a cost linked to the distance between f and f^g . Note that f is a vector polynomial in M variables of degree 2 with M components. In the following, \mathcal{E} takes the form

$$\mathcal{E}(f) = \frac{\langle \|e(f, t)\|_A^2 \rangle}{\langle \|e(f^g, t)\|_A^2 \rangle}, \quad (10)$$

where $\langle \cdot \rangle$ is a linear time average operator (discrete or continuous, for instance an integral over $[0, T]$ or an arithmetic average on a subdivision of $[0, T]$), $\|\cdot\|_A$ is a norm of \mathbb{R}^M and e is an operator with values in \mathbb{R}^M . This operator will be defined so that the solution a to the Cauchy problem

$$(\mathcal{P}_f(a)) \begin{cases} \dot{a}(t) = f(a(t)) \\ a(0) = a^e(0) \end{cases} \quad (11)$$

is a^e over $[0, T]$ if, and only if, $\|e(f, t)\|_A = 0$ for all $t \in [0, T]$. In fact, the i th component of $e(f, t)$ quantifies a distance linked to the i th POD mode between the data and the ODE system defined by f at the time t : it depends only on quantities related to the i th mode as $a_i^e, \dot{a}_i^e, f(a^e)$ or $f(a)$ for a satisfying $(\mathcal{P}_f(a))$. Note that $A \in \mathbb{R}^{M \times M}$ denotes the symmetric definite positive matrix associated to $\|\cdot\|_A$:

$$\forall z \in \mathbb{R}^M \quad \|z\|_A = \sqrt{z^T A z}. \quad (12)$$

Changing this matrix enables us to give more or less importance to certain POD components (see the remark below).

Three choices for e are proposed: a constrained non-linear definition (Section 3.3.1) and two definitions which are affine with respect to f (Sections 3.3.2 and 3.3.3). Appendix B emphasizes the fact that, for e affine, \mathcal{E} is a quadratic function and then the optimization problem reduces to a linear system.

\mathcal{D} is expressed using a semi-norm $\|\cdot\|_\Pi$ on the polynomial vector space:

$$\mathcal{D}(f) = \frac{\|f - f^g\|_\Pi^2}{\|f^g\|_\Pi^2}. \quad (13)$$

If $y \in \mathbb{R}^P$ is the vector of all the coefficients of the vector polynomial f of degree 2 in the natural monomial basis $\left(P = M\left(1 + M + \frac{M(M+1)}{2}\right) = \frac{M(M+1)(M+2)}{2}\right)$ $\|f\|_\Pi$ is defined by

$$\|f\|_\Pi = \sqrt{y^T \Pi y}, \quad (14)$$

where $\Pi \in \mathbb{R}^{P \times P}$ is a non-negative symmetric matrix. Modifying $\|\cdot\|_\Pi$, that is Π , changes the relative importance of each polynomial coefficient, in particular $\|f\|_\Pi$ may be restricted to a subset of the polynomial coefficients of f such that only this subset is taken into account (partial-Galerkin method, Sections 3.4 and 4.3). The semi-norms $\|\cdot\|_\Pi$ used in Section 4 are Euclidian norms of all or, respectively, a subset of the polynomial coefficients along the natural monomial basis: Π is the identity matrix I_P of dimension P or, respectively, I_P whose some chosen diagonal elements are set to zero.

Whatever the definition of e is, minimizing \mathcal{J}^α is a optimization problem in \mathbb{R}^P since it amounts to find the vector y^α of all the polynomial coefficients of f^α . The proposed methods amounts to adding a vector polynomial $f^\alpha - f^g$ to the original POD-Galerkin system. This polynomial can be virtually split into three polynomials: $f^\alpha - f^g = f^e + f^> + f^p$, that is into a small perturbation f^e which corrects the errors of the computation of f^g , a non-linear closure model $f^>$ of the truncated terms which is more general than a linear viscous model and, if the boundary conditions are not explicitly taken into account and in consequence the pressure term poses problems, a polynomial f^p which models the boundary pressure term. Indeed, the calibrated POD-Galerkin system is $\dot{a}(t) = f^\alpha(a(t))$, that is virtually $\dot{a}(t) = (f^g + f^e)(a(t)) + f^>(a(t)) + f^p(a(t))$.

3.1.1. Remark

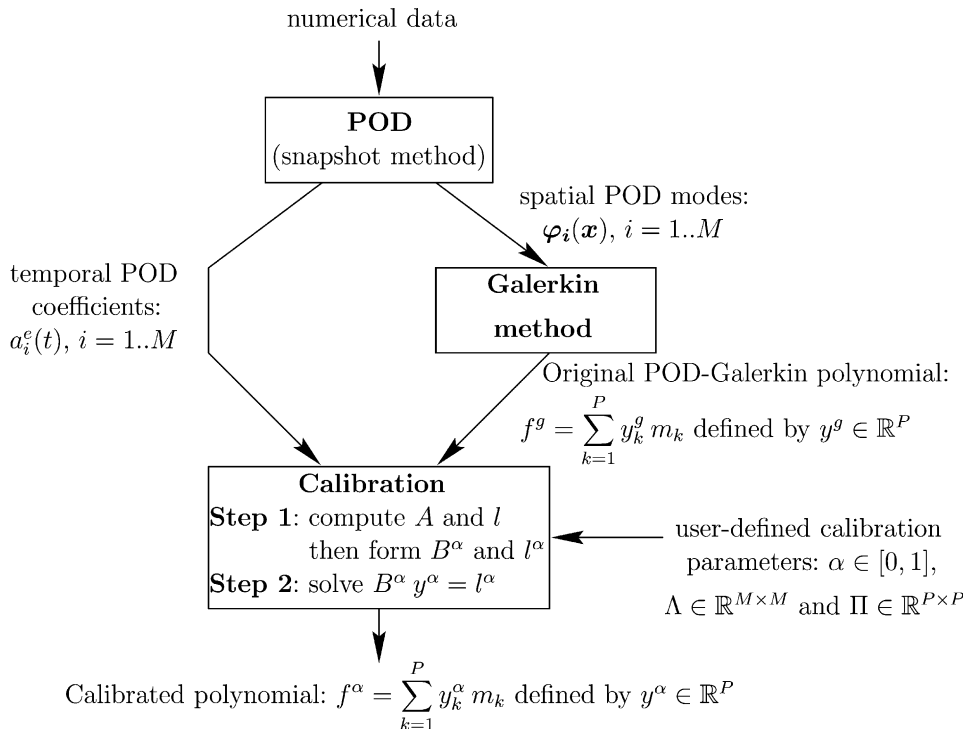
It is worth noting that the meanings of \mathcal{E} and \mathcal{D} depend on $\|\cdot\|_A$ and $\|\cdot\|_\Pi$ but also on the meaning of the time-dependent coefficients considered. For instance, in our numerical experiments (Section 4), $\|\cdot\|_A$ is the Euclidean norm (A is the identity matrix I_M of dimension M) hence it keeps the natural hierarchy of the POD modes: since the φ_i are normalized, $T^{-1} \int_0^T a_i^e(t)^2 dt = \sigma_i^2$ is the kinetic energy associated to the i th mode and the a_i^e are “naturally ranked”. For the same definitions of \mathcal{E} and \mathcal{D} , the interpretation of the results would not be equivalent for polynomial ODE systems constructed to approach the behaviour of the normalized time-dependent coefficients a_i^e/σ_i instead of the a_i^e (A should be changed into $\text{diag}(\sigma_1, \dots, \sigma_M)$ for \mathcal{E} to be equivalent).

Furthermore, it is better to calibrate the ODE system whose time-dependent unknowns are the a_i instead of the equivalent one whose unknowns are the a_i/σ_i for the same diagonal matrices $\|\cdot\|_A$ and $\|\cdot\|_\Pi$ since then minimizing \mathcal{E} amounts to decrease the distance between the ODE system and the data for the first modes in priority and since then it appears less expensive to modify in priority the polynomial coefficients of the last modes if you pay attention to the term \mathcal{D} .

However, in our numerical experiments, each component of the optimal vector polynomial f^α is computed independently of the others in practice owing to the particular choices of e , A and Π retained (see the introduction of Section 4). Thus, calibrating either POD-Galerkin systems is equivalent, yet the values of \mathcal{E} and \mathcal{D} are more representative of the effects of the calibrations for the POD-Galerkin system whose unknowns are the a_i .

3.2. Synthetic scheme of the calibration POD-Galerkin methods

To give a better idea of the proposed algorithms, the main steps of the calibration POD-Galerkin modelling for an affine definition of $e(\cdot, t)$ are here summed up:



The calibration methods optimize the coefficients of the quadratic vector polynomial f^g associated the reduced-order POD-Galerkin system. The problem is solved in \mathbb{R}^P by considering the P coefficients of the vector polynomials with M components of degree 2 in M variables: y^g and y^α are the vectors of the coefficients of f^g and f^α in the natural monomial basis (m_k).

If $e(f,t)$ is affine with respect to f then the calibration amounts to solve a linear system whose matrix B^α and right-hand side l^α are formed after the computation of the matrix $A = B^0$ and the right-hand side $l = l^0$ ($\alpha = 0$), which is performed during the two steps of the calibration: see Appendix B. The step 1 of the calibration, that is the computation of A and l , depends on the definition of the operator e thus is different for the two methods which are proposed in the following. For both of these methods, some expressions of A and l are given in Appendix C, moreover the linear systems which are obtained are detailed in the case $M = 2$ in Appendix D.

3.3. Three definitions for e

3.3.1. Non-linear definition with dynamical constraints

Since the main objective is to obtain an ODE system whose simulation recovers as accurately as possible the evolution of the data, the natural mathematical formulation of the problem would consist in defining $e(f,t)$ as

$$e_1(f,t) = a^e(t) - a(t), \quad (15)$$

under the constraint that $a(t)$ satisfies (11). Thus, a solution f^α to problem (9) would minimize the gap between data and dynamical system states on average.

Unfortunately, that strongly non-linear definition of e is not satisfactory for several reasons. Indeed, since polynomials f may not be globally Lipschitz (only locally), the unique maximal solution $a(t)$ to the Cauchy problem $(\mathcal{P}_f(a))$ can take infinite values in finite time, in particular before the final time T of the experiment. Thus, in general, $\langle \|e_1(f,t)\|_A^2 \rangle$ is not defined on all the vector polynomial space but only on an open subset \mathcal{O} (to which at least the polynomials of degree 1 belong): therefore, for $e = e_1$, $\mathcal{J}^\alpha(f)$ is not defined if $f \notin \mathcal{O}$. Notice that \mathcal{E} , as defined in Section 3.1, has no sense if $f^g \notin \mathcal{O}$ (case where the POD-Galerkin model is unstable). Furthermore, the minimization problem for $e = e_1$ is not well posed: several solutions coexist in general.

However, since \mathcal{J}^α takes finite values and is differentiable in \mathcal{O} , it would be possible to look for a local minimum, starting from $f = f^g$ (or from its linear part and redefining \mathcal{E} using for instance $e(0,t)$ instead of $e(f^g,t)$ if $f^g \notin \mathcal{O}$) and applying a non-linear conjugate gradient algorithm. But the computational cost of the gradient evaluation is large, the convergence is not guaranteed and the algorithm has to be designed in considering that a polynomial iterate is not necessary in \mathcal{O} . This non-linear definition of e can yet be modified into an affine one by suppressing the dynamical constraint (11) in the definition of e_1 as proposed in the next section.

3.3.2. State calibration method

The operator e_1 defined in the preceding section can be written

$$e_1(f,t) = a^e(t) - a^e(0) - \int_0^t f(a(\tau))d\tau, \quad (16)$$

where $a(t)$ is given by the constraint (11) on f . To suppress this non-linear constraint we can use:

$$e_2(f,t) = a^e(t) - a^e(0) - \int_0^t f(a^e(\tau))d\tau. \quad (17)$$

In this manner, we test how accurately the data respect the dynamical system, keeping the same point of view than in the previous section where the data history a^e and the state a of the solution to the ODE system defined by f are compared. Clearly the operator e_2 is affine with respect to f : minimizing \mathcal{J}^α gives rise to a linear system.

3.3.3. Flow calibration method

Since the ideal polynomial should satisfy $\dot{a}^e(t) = f(a^e(t))$, we propose as third choice for e the operator

$$e_3(f, t) = \dot{a}^e(t) - f(a^e(t)). \quad (18)$$

Therefore we try to minimize the gap between the dynamics of the data and the flow of the ODE system defined by f , that is the gap between the time derivative of a^e and the vector field defined by f along the trajectory covered by $a^e(t)$ for $t \in [0, T]$. In fact, e_3 is the time derivative of e_2 :

$$e_2(f, t) = \int_0^t e_3(f, \tau) d\tau \quad (19)$$

and e_3 is affine with respect to f as e_2 is.

3.4. Computational cost and partial-Galerkin method

The computational cost of the POD-Galerkin polynomial coefficients is large for transitional or turbulent flows. Indeed, if the flow structures cover a large range of scales, the number of POD modes kept to construct the ODE system and also the number of meshes are large. Moreover, the use of the calibration methods to improve the system increases that cost. However, we expect to be able to decrease the cost of the ODE system computation by “mixing” the Galerkin method with a calibration method, that is by calculating only a “minimum” number of POD-Galerkin polynomial coefficients then evaluating the others by the optimization process (see below).

If that technique is effective, its cost is likely to be smaller than the one of a full Galerkin method: the methods we propose only require the temporal information given by the POD (that is $a^e(t)$), whereas the Galerkin method uses the voluminous spatial information (the φ_i) and leads to spatial operations which are computationally expensive.

And yet, even if the cost of computing a POD-Galerkin system from a POD decreases, it is hard to predict whether the global cost, including the POD, will increase or not when that technique we call partial-Galerkin method is used. Indeed, when the snapshot method is applied to form the POD (see [13]), it is often possible to calculate a suitable set of POD modes from only few snapshots regularly distributed in time. In that case, the $a_i^e(t)$ are only calculated at the corresponding times during the POD computations (they are the eigenvectors of the temporal correlation matrix used to form the φ_i). Thus, it may be necessary to increase the computational cost of the POD to have enough temporal data for the partial-Galerkin methods to be effective. It is noticeable that the number of temporal POD data (the number of times at which a^e is known) could be artificially increased using cubic spline interpolation.

Nevertheless, that technique remains interesting since this is expected to decrease the computational cost of the calibration POD-Galerkin methods.

Once a subset of the polynomial coefficients have been evaluated by the Galerkin method, two strategies are considered. In all cases, the initial polynomial Galerkin polynomial f^g is defined by setting the other coefficients to zero.

The first strategy is to define $\|\cdot\|_\Pi$ as a semi-norm which takes only the subset of the coefficients computed by the Galerkin method into account. For example, when this strategy is applied in our numerical experiments, Π is defined as the modified identity matrix whose diagonal values whose locations correspond to the coefficients which were not computed are set to zero.

The second strategy is to use a definite norm $\|\cdot\|_\Pi$ on all the coefficients (for example $\Pi = I_P$ as in our experiments). In that latter case, it is a priori important to compute by the Galerkin method the polynomial coefficients whose effects cannot be neglected since the others will be assumed to be zero and taken into account in $\|f - f^g\|_\Pi$.

Some numerical results of partial-Galerkin methods are discussed in Section 4.3.

4. Numerical experiments

In this section, some results for the two calibration methods ($e = e_2$ and e_3) are presented for the fluid flow configurations of Sections 2.2 and 2.3.

$\|\cdot\|_\Lambda$ is the usual Euclidian norm on \mathbb{R}^M ($\Lambda = I_M$). Moreover, all the results plotted here were computed with $\Pi = I_P$ (so $\|\cdot\|_\Pi$ is the complete Euclidian norm on the monomial basis). Only the experiments based on the first strategy of partial-Galerkin methods were performed with some singular matrices Π (some of its diagonal elements are set to zero as explained in the previous section), however no results are plotted in this case because the linear system is ill-conditioned: read the Section 4.3 for the details.

It is worthy of note that for the state and flow calibrations ($e = e_2$ or $e = e_3$) and for the particular forms of Λ and Π used, the resulting linear problem can be naturally split into M similar linear problems thus it requires to solve a linear problem of dimension P/M with M different right-hand sides (where $P/M = \frac{(M+1)(M+2)}{2}$ is the dimension of the scalar polynomial space of degree 2): each component f_i^α of the optimal polynomial can be computed independently of the others (this is emphasized in Appendix D for $M = 2$).

We remind you that the optimal solution computed is a vector $y^\alpha \in \mathbb{R}^P$ which defines all the coefficients of a vector polynomial f^α of degree 2: all the coefficients are calibrated in this way, even if only a part of the POD-Galerkin coefficients is computed and taken into account (partial-Galerkin methods).

For the flow calibration ($e = e_3$), $\langle \cdot \rangle$ is the arithmetic time average on the regular subdivision of $[0, T]$ corresponding to the snapshot database used:

$$\langle g(t) \rangle = \frac{1}{N} \sum_{k=0}^{N-1} g(k\Delta t) \quad \text{with } \Delta t = \frac{T}{N-1}. \quad (20)$$

For the state calibration ($e = e_2$), $\langle \cdot \rangle$ is defined by the discretization of the integration over $[0, T]$ given by the trapezoidal rule (second-order method), which almost amounts to use an arithmetic time average:

$$\langle g(t) \rangle = \frac{\Delta t}{T} \sum_{k=0}^{N-1} \frac{1}{2} [g(k\Delta t) + g((k+1)\Delta t)]. \quad (21)$$

The implementation of the state calibration method and the calculation of the corresponding cost function \mathcal{E} , denoted by \mathcal{E}_2 to precise that $e = e_2$, imply the discretization of terms in the form $\int_0^t g(a^\alpha(\tau)) d\tau$ and the same trapezoidal rule is applied (these appear in the expressions of A and l defined in Appendix C).

Moreover, all the simulations of the POD-Galerkin systems are performed by a classical fourth-order Runge-Kutta scheme with a time step of $10^{-4}T$, in particular to evaluate \mathcal{E} for $e = e_1$ (which is denoted by \mathcal{E}_1 in the following).

The numerical code was previously validated on data generated by some simulations of three-dimensional quadratic ODE systems: a prototype one proposed by Rössler in [17] and the Lorenz system (see [18,19]). Even for $\alpha = 0$, suitable calibrated systems f^α were obtained.

4.1. Numerical efficiency and impact on the POD-Galerkin systems

The optimal polynomials f^α and the cost functions \mathcal{E} are indexed by the subscript of the corresponding operator e : \mathcal{E}_1 for $e = e_1$, \mathcal{E}_2 and $f^{\alpha,2}$ for $e = e_2$, \mathcal{E}_3 and $f^{\alpha,3}$ for $e = e_3$: $f^{\alpha,2}$ is obtained by state calibration and $f^{\alpha,3}$ by flow calibration, respectively. More precisely, for all $j \in \{1,2,3\}$ and all $k \in \{2,3\}$,

$$\mathcal{E}_j(f) = \frac{\langle \|e_j(f, t)\|_A^2 \rangle}{\langle \|e_j(f^g, t)\|_A^2 \rangle}, \quad \text{in particular } \mathcal{E}_j(f^{\alpha,k}) = \frac{\langle \|e_j(f^{\alpha,k}, t)\|_A^2 \rangle}{\langle \|e_j(f^g, t)\|_A^2 \rangle}, \quad (22)$$

where $f^{\alpha,k}$ is the optimal polynomial which satisfies

$$(1 - \alpha)\mathcal{E}_k(f^{\alpha,k}) + \alpha\mathcal{D}(f^{\alpha,k}) \leqslant (1 - \alpha)\mathcal{E}_k(f) + \alpha\mathcal{D}(f) \quad (23)$$

for all vector polynomial f ($j = k$ in that latter equation): $f^{\alpha,k}$ depends on α .

The values of $\sqrt{\mathcal{E}_1(f^{\alpha,k})}$, $\sqrt{\mathcal{E}_2(f^{\alpha,k})}$, $\sqrt{\mathcal{E}_3(f^{\alpha,k})}$ and $\sqrt{\mathcal{D}(f^{\alpha,k})}$ are presented for both calibration methods, that is $k = 2$ or $k = 3$, applied to the two flow configurations with respect to α (or a parameter δ in increasing bijection with α on $[0,1]$, see below).

For $\alpha = 1$, if $\|\cdot\|_\Pi$ is a norm (not just a semi-norm), the unique solution to the minimization problem is $f^\alpha = f^g$, thus $\mathcal{D}(f^\alpha) = 0$ and $\mathcal{E}(f^\alpha) = 1$ since \mathcal{E} is a normalized cost: the POD-Galerkin is not calibrated. For state or flow calibration methods ($k = 2$ or $k = 3$), the original ODE system is more and more calibrated in the sense that $\sqrt{\mathcal{E}_k(f^{\alpha,k})}$ decreases and more and more modified in the sense that $\sqrt{\mathcal{D}(f^{\alpha,k})}$ increases as α tends to zero: see (23). It is noticeable that, if $\sqrt{\mathcal{E}_2(f^{\alpha,2})}$, $\sqrt{\mathcal{E}_3(f^{\alpha,3})}$, $\sqrt{\mathcal{D}(f^{\alpha,2})}$ and $\sqrt{\mathcal{D}(f^{\alpha,3})}$ are necessary monotone functions of $\alpha \in [0,1]$ by definition, the curves of $\sqrt{\mathcal{E}_1(f^{\alpha,2})}$, $\sqrt{\mathcal{E}_1(f^{\alpha,3})}$, $\sqrt{\mathcal{E}_2(f^{\alpha,3})}$ and $\sqrt{\mathcal{E}_3(f^{\alpha,2})}$ may be non-monotone a priori.

Few components of the solutions to the original system defined by f^g and of some calibrated systems, which are necessary computed to evaluate \mathcal{E}_1 , are displayed in the following (in phase-portrait format for the square-cylinder flow configuration and in function of the time for the step flow configuration): a_i^g is the i th component of the solution a^g to the original POD-Galerkin system and $a_i^{\alpha,k}$ denotes the i th component of the solution $a^{\alpha,k}$ to the calibrated system defined by $f^{\alpha,k}$. For instance, $a^{1,2}$ and $a^{1,3}$ are respectively the solutions to the state- and flow-calibrated systems computed with $\alpha = 1$: $a^{1,2} = a^{1,3} = a^g$ if $\|\cdot\|_\Pi$ is definite (Π non singular).

4.1.1. The square-cylinder configuration

The results were computed varying linearly α , but also varying linearly a parameter δ such that

$$\alpha = \frac{\delta}{\zeta(1 - \delta) + \delta} \quad \text{with } \zeta = \frac{\langle \|e(f^g, t)\|_A^2 \rangle}{\langle \|e(0, t)\|_A^2 \rangle}, \quad (24)$$

α is in increasing bijection with δ on $[0,1]$. In fact, that second way to vary α amounts to minimize

$$\tilde{\mathcal{J}}^\delta(f) = (1 - \delta)\tilde{\mathcal{E}}(f) + \delta\mathcal{D}(f), \quad (25)$$

with

$$\tilde{\mathcal{E}}(f) = \zeta\mathcal{E}(f) = \frac{\langle \|e(f, t)\|_A^2 \rangle}{\langle \|e(0, t)\|_A^2 \rangle}, \quad (26)$$

since

$$\tilde{\mathcal{J}}^\delta(f) = \frac{\delta}{\alpha}\mathcal{J}^\alpha(f) = [\zeta(1 - \delta) + \delta]\mathcal{J}^\alpha(f). \quad (27)$$

Indeed, results with linear variation of δ are more readable than ones with linear variation of α since the curves decrease or increase extremely rapidly when α varies between 0.95 and 1 as you can see in Fig. 10. Therefore, two series of results are obtained and plotted for α and δ in $\{0.05, 0.1, \dots, 1\}$. α is displayed in function of δ for $e = e_2$ and $e = e_3$ in Fig. 9 for $\delta \in [0.05, 1]$. The minimization results are presented in Fig. 10. It is observed that $\sqrt{\mathcal{E}_1(f^{\alpha,2})}$, $\sqrt{\mathcal{E}_3(f^{\alpha,2})}$ and $\sqrt{\mathcal{E}_1(f^{\alpha,3})}$ are increasing functions of α . Only $\sqrt{\mathcal{E}_2(f^{\alpha,3})}$ decreases very slowly for $\delta \in [0.05, 0.25]$ but its global shape is an increase.

For both calibrations ($k = 2$ or $k = 3$), $\sqrt{\mathcal{E}_3(f^{\alpha,k})}$ appears little reduced for small values of α ($\sqrt{\mathcal{E}_3(f^{\alpha,2})}$ and $\sqrt{\mathcal{E}_3(f^{\alpha,3})}$ are about 0.89 for $\alpha = 0.05$): this is normal since the non-calibrated POD-Galerkin system f^g was relatively accurate (the difference between a^e and $f^g(a^e)$ which defines $e_3(f^g, t)$ is very small, look at the Fig. 4) and since the efficiency of the calibration is limited by the machine precision.

The main observation is that $\sqrt{\mathcal{E}_1(f^{\alpha,k})}$ vanishes for $k = 2$ and $k = 3$ as well when α tends to zero: state and flow calibrations are effective on this two-dimensional quasi-incompressible configuration. Moreover, this can be done for very small perturbations of the original POD-Galerkin system since, for instance, $\sqrt{\mathcal{D}(f^{\alpha,2})}$ and $\sqrt{\mathcal{D}(f^{\alpha,3})}$ are less than 2% and correspond to very good improvements of the ODE system for $\alpha = 0.95$: $\sqrt{\mathcal{E}_1(f^{\alpha,2})}$ and $\sqrt{\mathcal{E}_1(f^{\alpha,3})}$ are about 0.07.

To visualize the effectiveness of the calibration of the POD-Galerkin system of the square–cylinder flow, the solution a^g to the non-calibrated system is presented over three periods, that is for $t \in [0, 3T]$, with the solution $a^{0.05,3}$ to the system obtained by flow calibration with $\alpha = 0.05$ in Fig. 11. It is observed that the calibrated system gives a solution which is periodic (and matches the data history a^e) whereas the solution given by the original POD-Galerkin system diverges from that periodic trajectory.

4.1.2. The backward-facing-step configuration

For the second test flow configuration, the calibration of two POD-Galerkin systems are experimented: the 86-mode system and the 45-mode system. The 45 first POD modes capture more than 95% of the fluctuant kinetic energy of the data; the polynomial coefficients of the 45-mode system are included in the coefficients of the 86-mode system.

Some results for $\alpha = 0.001$ and α in $\{0.05, 0.1, \dots, 1\}$ are plotted: see Figs. 12 (86-mode system) and 13 (45-mode system). For the two original POD-Galerkin systems, it is observed that $\sqrt{\mathcal{E}_1(f^{\alpha,2})}$, $\sqrt{\mathcal{E}_3(f^{\alpha,2})}$, $\sqrt{\mathcal{E}_1(f^{\alpha,3})}$ and $\sqrt{\mathcal{E}_2(f^{\alpha,3})}$ are increasing functions of α ; furthermore, $\sqrt{\mathcal{E}_1(f^{\alpha,k})}$, $\sqrt{\mathcal{E}_2(f^{\alpha,k})}$ and $\sqrt{\mathcal{E}_3(f^{\alpha,k})}$ take very small values for $\alpha = 0.001$ for both calibration methods ($k = 2$ or $k = 3$).

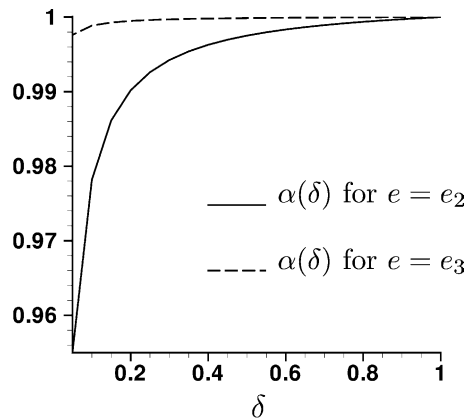


Fig. 9. α function of δ .

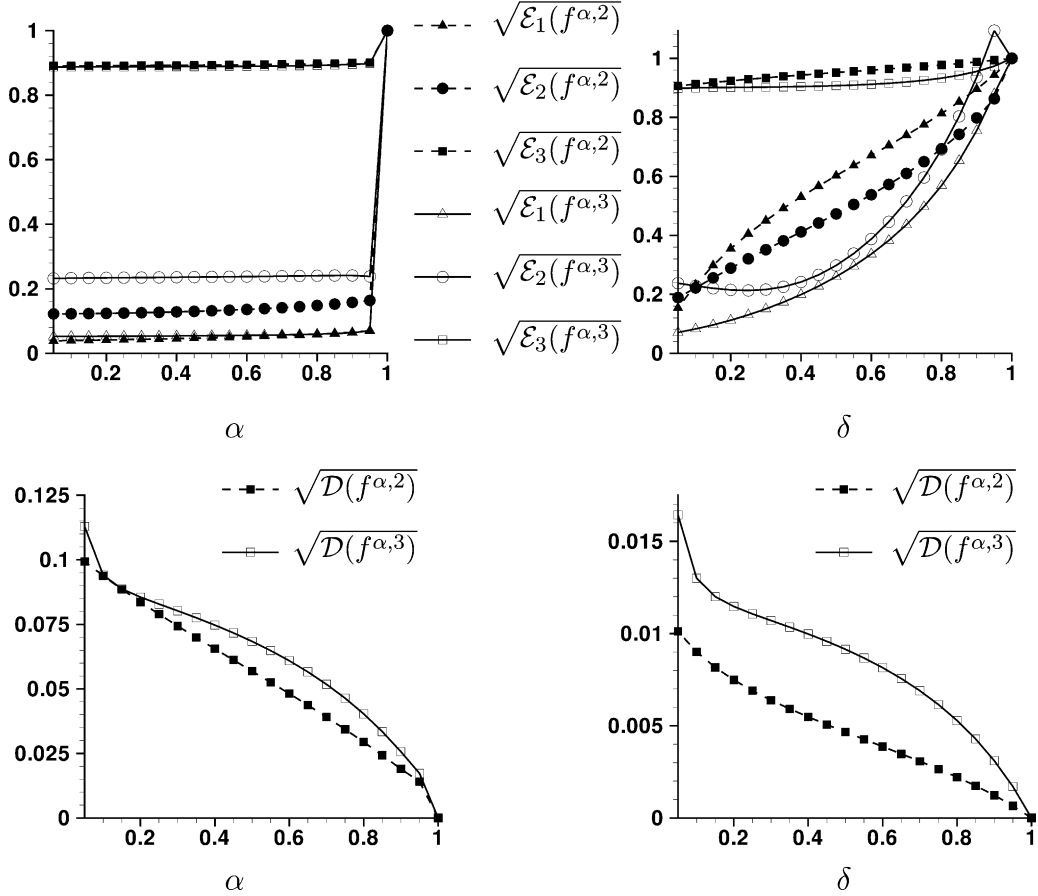


Fig. 10. Minimization results for the square-cylinder configuration.

So the calibrations are effective but the optimal polynomials $f^{\alpha,2}$ and $f^{\alpha,3}$ cannot be regarded as small perturbations of the original POD-Galerkin system f^g for small values of α any more. For instance, for $M = 86$ or $M = 45$, $\sqrt{\mathcal{D}(f^{\alpha,k})}$ reaches about 0.2 when $\sqrt{\mathcal{E}_1(f^{\alpha,k})}$ is around 0.25 for both methods ($k = 2$ or $k = 3$). For $\alpha = 0.001$, the ODE system is more modified for $M = 45$ than for $M = 86$ (the values of \mathcal{D} are greater for $M = 45$), which was expected since more truncated terms have to be modeled.

Furthermore, notice there is a gap between the formal expressions of f^g and the nature of the data used since the data were computed using a finite-difference large-Eddy scheme and the boundary term $T_{\partial\Omega}$ was neglected in the variational formulation (see Section 2.1 and Appendix A): the calibration methods have to model the truncated terms but also to fill this gap.

To display the effects of the calibrations of the 86-mode system, few components of the systems calibrated with $\alpha = 0.95$ or $\alpha = 0.05$ are plotted with the corresponding components of a^g and a^e .

Fig. 14 presents some components relative to three of the ten first POD modes. For both methods ($k = 2$ and $k = 3$), $a_i^{\alpha,k}$ converges as expected to a_i^e as α tends to zero, for the three indexes $i = 1, 5$ and 10 : the relative difference $(T\sigma_i)^{-1} \int_0^T (a_i^e(t) - a_i^{\alpha,k}(t))^2 dt$ decreases, moreover $a_i^{\alpha,2}$ and $a_i^{\alpha,3}$ match a_i^e for $\alpha = 0.05$.

Some components with larger indices, corresponding to less energetic POD modes, are displayed in Fig. 15. It appears that the histories of $a_{40}^{0.05,k}$, $a_{60}^{0.05,k}$ and $a_{80}^{0.05,k}$ are very satisfying for $k = 2$ and $k = 3$ as well, even

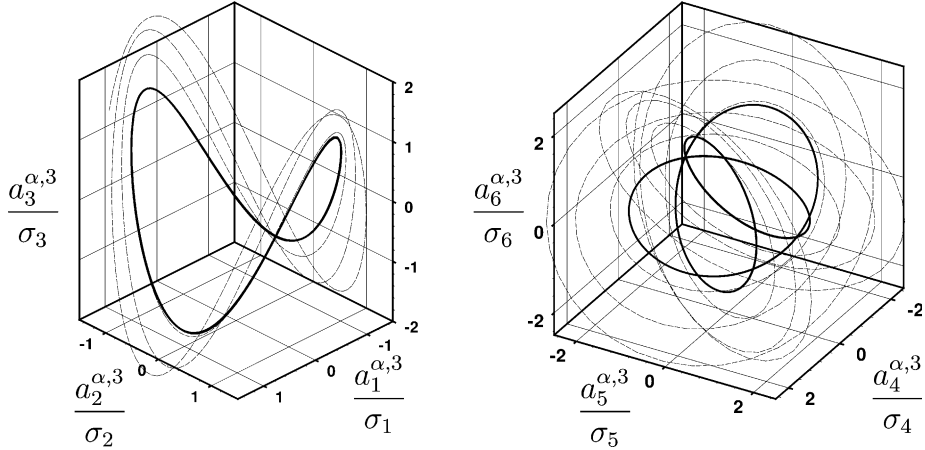


Fig. 11. Solution $a^g = a^{1,3}$ ($\alpha = 1$) to the non-calibrated system (thin dashed line) and solution $a^{0.05,3}$ to the system calibrated with $\alpha = 0.05$ by the flow method (thick line) for $t \in [0, 3T]$.

if $a_i^{0.05,2}$ and $a_i^{0.05,3}$ do not match perfectly a_i^e for $i = 60$ and $i = 80$: the calibrations succeed in modelling the main effects of the truncated POD modes.

4.2. Remark on condition numbers

Some computations were also performed with $\alpha = 0$ for the preceding POD-Galerkin systems and for both calibration methods. In those cases, the methods failed to compute a numerically stable ODE system although it was possible for the Rössler and Lorenz systems: taking f^g into account seems compulsory in practice when the number of modes is not very small. This phenomenon can be understood looking at the condition numbers of the matrices of the linear systems. The linear systems are indeed ill-conditioned for $\alpha = 0$ and \mathcal{D} is necessary to form a non-singular problem whose an approximate solution can be computed.

The base-10 logarithm of the condition numbers $\mathcal{K}(B^\alpha)$ of the matrices B^α formed during the calibrations (see Appendix B) is plotted as a function of α in Fig. 16 for the 6-mode model of the square–cylinder

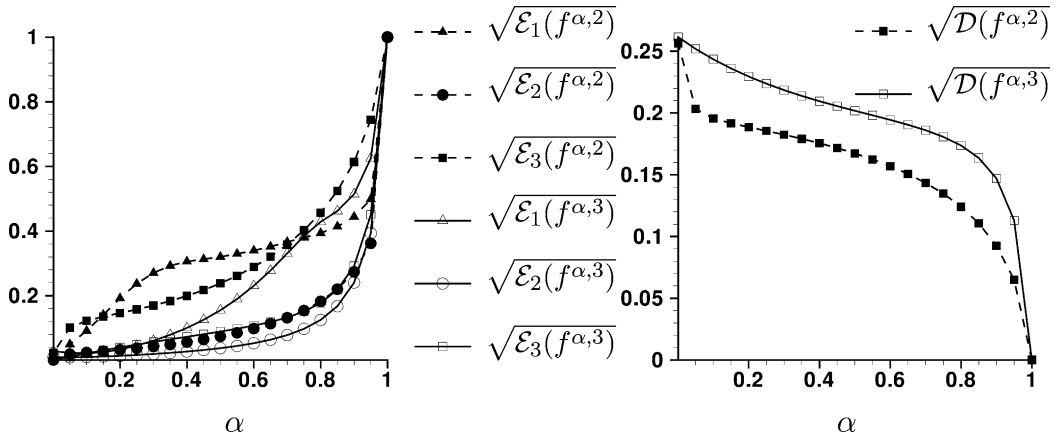


Fig. 12. Minimization results for the 86-mode POD-Galerkin system of the backward-facing-step configuration ($M = 86$).

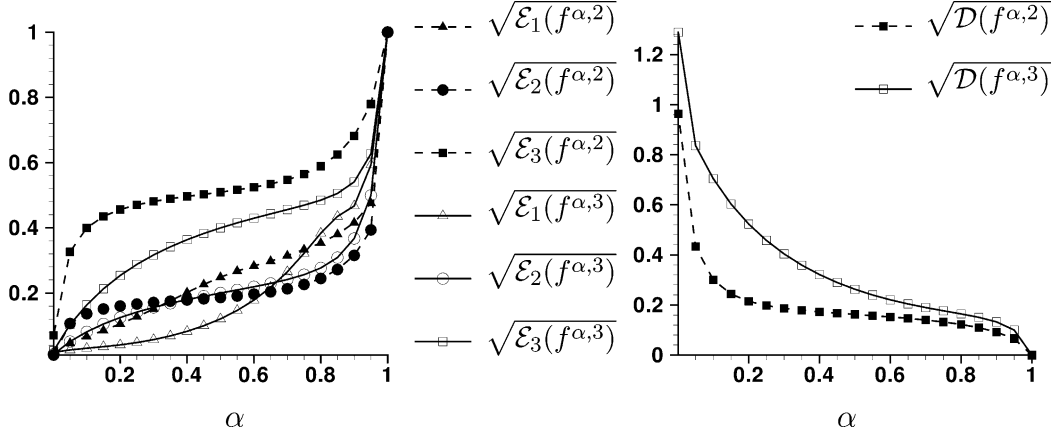


Fig. 13. Minimization results for the 45-mode POD-Galerkin system of the backward-facing-step configuration ($M = 45$).

configuration (left) and for the 86-mode model of the backward-facing step configuration (right). It gives estimates of how many base-10 digits are lost when the corresponding linear systems are solved.

The numerical experiments presented were performed by manipulating 64-bit double precision numbers, that is about 15 significative decimal digits, and by using a direct method to solve the linear system. Here, $\log_{10}(\mathcal{K}(B^0))$ is always greater than 15: the problem becomes ill-conditioned for $\alpha = 0$.

4.3. Partial-Galerkin methods

In this section, the partial-Galerkin methods are experimented from the Galerkin polynomial coefficients of the 86-mode system of the backward-facing step configuration. All the constant and linear monomials evaluated by the Galerkin method are taken into account but only a subset of the numerous quadratic ones. If the calibration methods remain effective for a small subset, considering that the other coefficients are zero or defining $\|\cdot\|_\Pi$ so that only this subset matters, a computational gain is then obtained and that gain may be greater than the increase of the cost of the POD computations which would be necessary for the calibrations to be effective (see Section 3.4).

The quadratic terms which are neglected are chosen keeping in mind that the interactions between POD modes are local, hence the “non-local” polynomial coefficients little matter a priori. That idea is based on the observations made in [20,8]. More precisely, if $C_j^{i_1, i_2} a_{i_1} a_{i_2}$ denotes the quadratic monomials of the j th component of a vector polynomial f as in Eq. (6), the monomial $C_j^{i_1, i_2} a_{i_1} a_{i_2}$ is neglected if, and only if, $|i_1 - i_2|$ is strictly greater than a threshold k . This criterion is the same for all the components of f (it does not depend on j) thus the calibration method still amounts to solving a linear problem of dimension P/M with M different right-hand sides, as in the previous experiments (as precised in the beginning of Section 4). Notice that more sophisticated criterions with dependence on j could be proposed (for instance $\min(|i_1 - j|, |i_2 - j|) > k_j$ for M thresholds k_j): these would be closer to the studies of the locality of the kinetic energy transfers of [20,8], nevertheless only the first criterion was tested for practical considerations.

Firstly, semi-norms $\|\cdot\|_\Pi$ can be defined so that only the chosen subset of coefficients are taken into account: this is the first strategy where some diagonal elements of Π are set to zero as explained at the end of Section 3.4. In that way, the methods do not implicitly assume that the neglected Galerkin coefficients are zero.

Unfortunately, this choice is not robust, since it generally leads to ill-conditioned linear systems. Indeed, when $\|\cdot\|_\Pi$ is not definite, the linear system is singular for $\alpha = 1$, whereas it seems that the contribution of \mathcal{D}

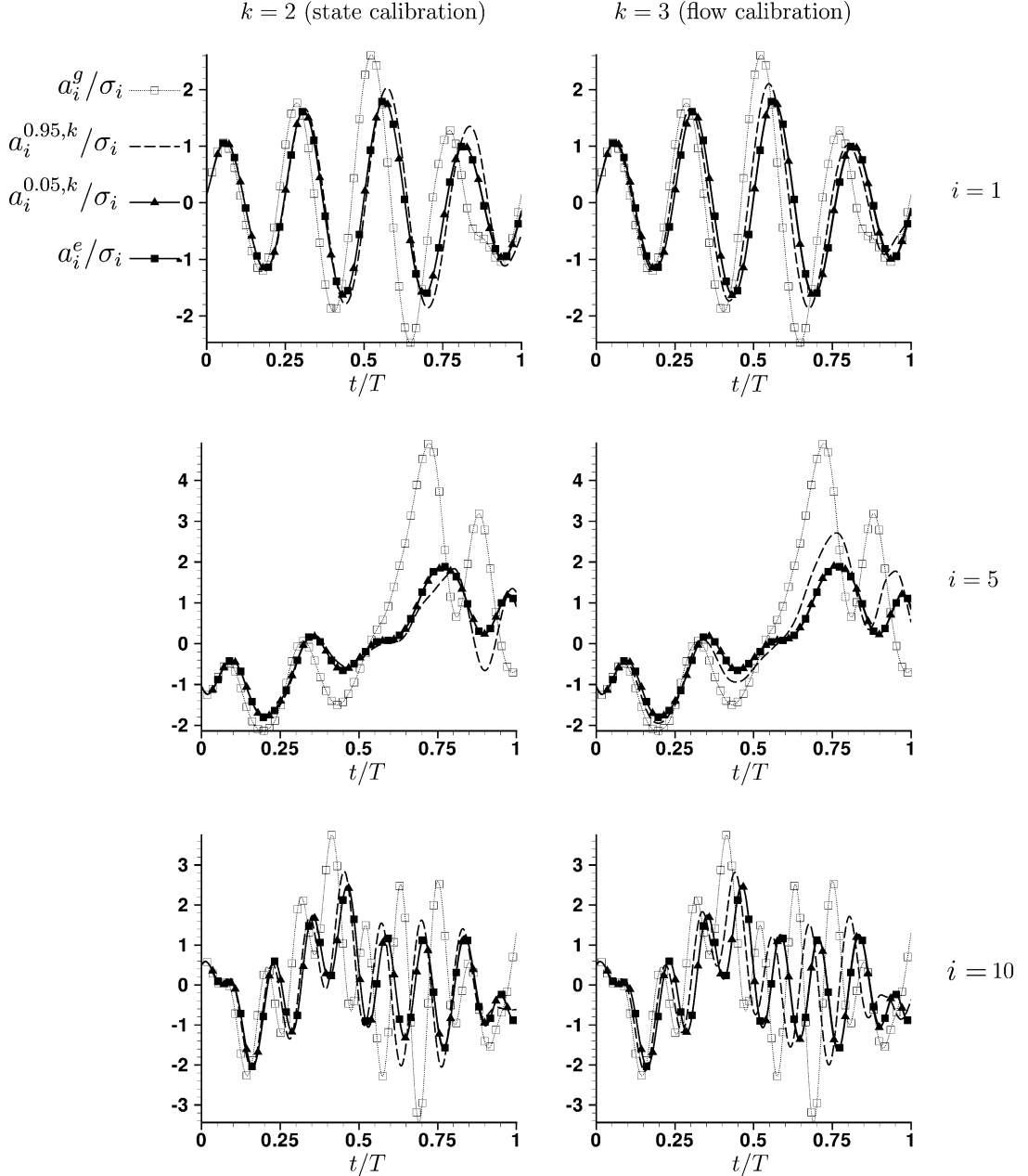


Fig. 14. i th components of the solutions a^g to the original POD-Galerkin system and $a^{\alpha,k}$ to systems calibrated with $\alpha = 0.95$ and $\alpha = 0.05$ by state ($k = 2$) or flow ($k = 3$) method and i th component of the data history a^e , for $i = 1, 5$ and 10 .

improves the condition number in the previous experiments (Section 4.2). In consequence, k must be close to M in our experiments for the calibrated system to be numerically stable and accurate.

Secondly, $\|\cdot\|_{\Pi}$ is defined as the definite Euclidian norm of the polynomial coefficients along the natural monomial basis and the neglected Galerkin coefficients are assumed to be zero in the definition of f^g . Some

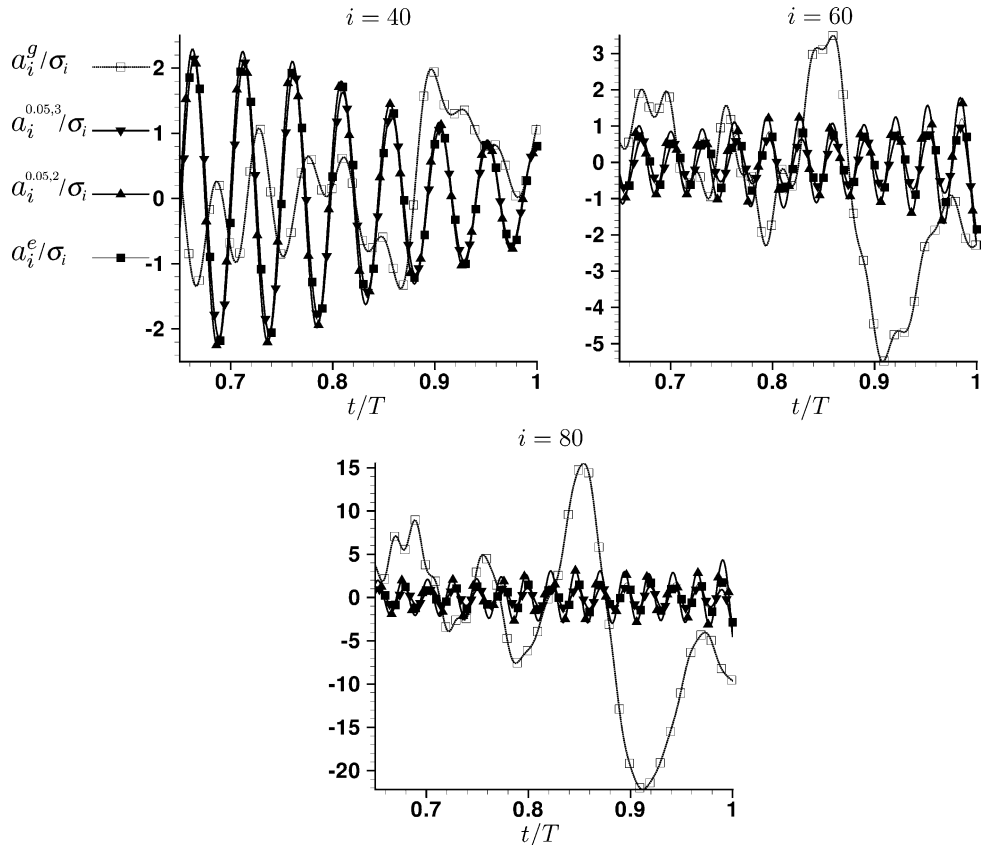


Fig. 15. 40th, 60th and 80th components of the data history a^e , of the solution a^g to the original system and of the solutions $a^{0.05,2}$ and $a^{0.05,3}$ to the state- and flow-calibrated systems for $t \in [0.65T, T]$.

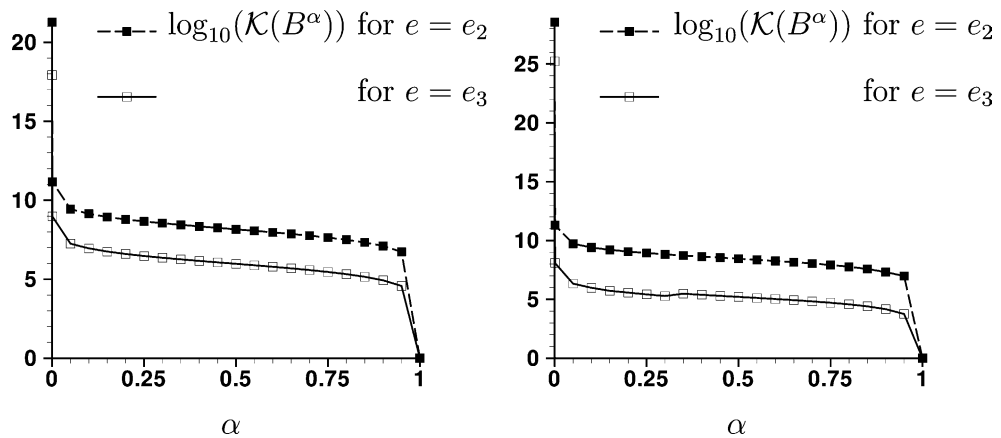


Fig. 16. Condition numbers obtained during the calibrations of the 6-mode system of the square-cylinder flow (left) and of the 86-mode system of the backward facing-step flow (right) for $\alpha = 0.001$ and α in $\{0.05, 0.1, \dots, 1\}$.

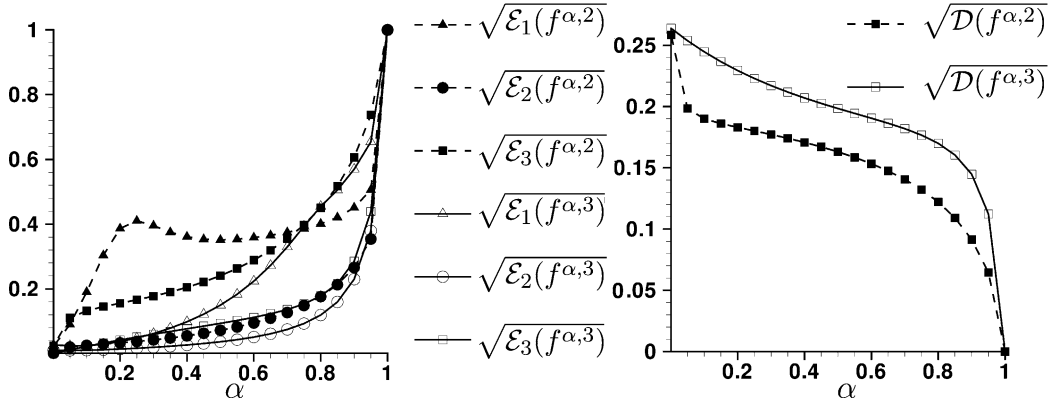


Fig. 17. Minimization results for the partial 86-mode system of the backward-facing-step flow corresponding to a threshold $k = 40$.

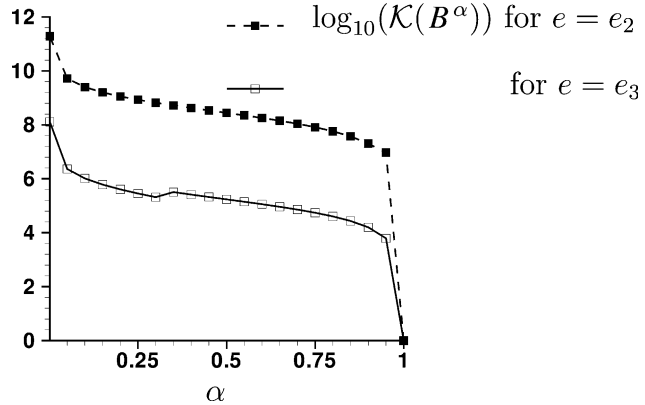


Fig. 18. Condition numbers obtained from the partial 86-mode system of the backward facing-step configuration corresponding to a threshold $k = 40$.

numerical experiments based on this second strategy were performed from the partial 86-mode Galerkin system corresponding to $k = 40$ for $\alpha = 0.001$ and α in $\{0.05, 0.1, \dots, 1\}$.

The results appear satisfying since relatively close to the preceding ones obtained from the full 86-mode Galerkin system; see Fig. 17. Moreover the conditions numbers, plotted in Fig. 18, are not worse than before.

All this leads to conclude that, in the case of transitional or turbulent flow modelling, the partial-Galerkin methods are interesting alternatives for correcting automatically the reduced-order POD-Galerkin system behaviour at relatively low cost, assuming that non-local POD interactions are negligible and using a definite norm $\|\cdot\|_{\Pi}$.

5. Conclusions

Two numerical methods which rely on minimization problems and give rise to linear systems were proposed to improve reduced-order POD-Galerkin systems by calibrating their polynomial coefficients. They

can be applied to unstable POD-Galerkin systems, that is systems which take infinite values before the time bound T considered. These methods exploit the temporal part of the POD information which is not taken into account in the POD-Galerkin approach.

Some numerical tests were performed on a relevant problem using 1000 velocity snapshots of a three-dimensional turbulent flow: the numerical behaviours of the 86-mode and 45-mode POD-Galerkin systems of a backward-facing-step flow were noticeably improved by calibrating their polynomial coefficients.

The computational cost of the construction and resolution of the linear systems is reasonable for both calibration methods since this cost is generally less than the cost of the POD-Galerkin calculations for transitional or turbulent flows. However, although reasonable, the global cost of the calibration is not insignificant since more POD or interpolation computations could be necessary to increase the number of data for the methods to be accurate enough. In particular, the first method ($e = e_2$) needs close snapshots for the discretization of the integrals over $[0, t]$ to be accurate. Fortunately, large computational gain can be obtained using partial-Galerkin methods in the cases of transitional or turbulent flows.

This work suggests several points to investigate. First, physical interpretation of the calibrations obtained should be studied. Furthermore, the impact of this POD-Galerkin modelling with calibration for the active control of an unsteady flow remains unknown. Moreover, the methods could be immediately applied on compressible flow cases since polynomial POD-Galerkin systems can be derived from the Navier–Stokes equations for a perfect gas (see [11] or [5]). And eventually, the effectiveness of the calibration methods could be tested for other modelling problems, not necessary in the fluid mechanics field. Indeed, the methods can be easily extended to non-polynomial problems by assuming a new suitable space instead of the quadratic polynomial one which is considered here.

Appendix A. Treatment of the boundary conditions in the Galerkin method

The boundary term of the variational formulation (4) is

$$T_{\partial\Omega} = \int_{\partial\Omega} t_{\partial\Omega} ds \quad \text{with } t_{\partial\Omega} = \left(p\mathbf{n} - \frac{1}{Re} [\nabla u]\mathbf{n} \right) \cdot \boldsymbol{\varphi}, \quad (\text{A.1})$$

with p the pressure field and \mathbf{n} the outward unitary normal at the border $\partial\Omega$ of Ω . That natural flux $t_{\partial\Omega}$ of the incompressible Navier–Stokes equations can be fully defined on $\partial\Omega$ by \mathbf{u} for a large class of boundary conditions prescribed for incompressible flows. Thus, the pressure vanishes from the variational formulation and an ODE system only based on the POD of the velocity can be constructed by applying the Galerkin method.

Indeed, let us regard the following conditions on the boundary $\partial\Omega = \Gamma_D \cup \Gamma_N$ with $\Gamma_N = \partial\Omega \setminus \Gamma_D$:

$$\mathbf{u} = \mathbf{w} \quad \text{on } \Gamma_D, \quad (\text{A.2})$$

$$-\tilde{\sigma}\mathbf{n} = \boldsymbol{\beta} \quad \text{on } \Gamma_N, \quad (\text{A.3})$$

where

$$\tilde{\sigma} = \frac{1}{Re} [\nabla u] - pI_d \quad (\text{A.4})$$

is a pseudo stress tensor (I_d is the identity matrix of dimension d) and $\boldsymbol{\beta}$ the pseudo flow stress set on Γ_N . (A.3) is a generalization of some boundary conditions usually used in incompressible flow simulations to represent the flow in an unbounded region: for instance

$$[\nabla u]\mathbf{n} = 0 \quad \text{and} \quad p = q, \quad (\text{A.5})$$

which can be applied for external flow (q is the pressure which is prescribed on Γ_N) or

$$p\mathbf{n} - \frac{1}{Re}[\nabla u]\mathbf{n} = 0 \quad (\text{A.6})$$

(pseudo stress free condition) which is often used as outlet condition for canal flows: read [21] or [2].

If the Dirichlet condition on the velocity is nonhomogeneous, that is $\mathbf{w} \neq 0$ on Γ_D , the POD is performed on $\mathbf{u}^e - \bar{\mathbf{u}}^e$ with a solenoidal field $\bar{\mathbf{u}}^e$ satisfying $\bar{\mathbf{u}}^e = \mathbf{w}$ on Γ_D : the POD modes are then solenoidal and vanish on Γ_D as $\mathbf{u}^e - \bar{\mathbf{u}}^e$ and the test function φ has to be considered in a space of solenoidal functions which vanish on Γ_D . Therefore, $t_{\partial\Omega}$ takes zero values on Γ_D .

Moreover, the boundary condition (A.3) implies that $t_{\partial\Omega} = \boldsymbol{\beta} \cdot \varphi$ on Γ_N . Thus, the variational formulation (4) becomes

$$\frac{d}{dt}(\mathbf{u}, \varphi) + ((\mathbf{u} \cdot \nabla)\mathbf{u}, \varphi) + \frac{1}{Re} \sum_{i=1}^d (\nabla u_{x_i}, \nabla \varphi_{x_i}) + \int_{\Gamma_N} \boldsymbol{\beta} \cdot \varphi \, ds = (\mathbf{h}, \varphi). \quad (\text{A.7})$$

Finally, the POD-Galerkin system is obtained from (A.7) using the Galerkin method with the POD modes as test functions and basis functions for $\mathbf{u} - \bar{\mathbf{u}}^e$.

Notice that $T_{\partial\Omega} = \int_{\Gamma_N} \boldsymbol{\beta} \cdot \varphi \, ds = 0$ if $\boldsymbol{\beta} = -P\mathbf{n}$ with P a constant pressure for any solenoidal test function φ which is zero on Γ_D , which is logical since only the gradient of the pressure and not the pressure is physical in the case of an incompressible flow ($\nabla(p + P) = \nabla p$).

For the backward-facing step flow configuration, the outlet condition (A.6) is used. However, for the square-cylinder flow configuration, the outlet condition is little different: the transverse velocity u_{x_2} , the normal derivative of the streamwise velocity $\partial_{x_1} u_{x_1}$ and the dynamic pressure were set to zero during the computations at the outlet, that is

$$p\mathbf{n} - \frac{1}{Re}[\nabla u]\mathbf{n} = -P_s\mathbf{n} - \frac{1}{Re} \partial_{x_1} u_{x_2} \mathbf{x}_2 \quad (\text{A.8})$$

at the outlet, where P_s is a constant static pressure, \mathbf{x}_2 is the unitary vector in the transverse direction, the subscripts x_1 and x_2 denote respectively the streamwise and transverse components ($n_{x_1} = 1$ and $n_{x_2} = \mathbf{n} \cdot \mathbf{x}_2 = 0$ at the outlet) and where $\partial_{x_1} u_{x_2}$ is the derivative of $u_{x_2} = \mathbf{u} \cdot \mathbf{x}_2$ in the normal direction. That condition is not strictly equivalent to (A.3) for $\boldsymbol{\beta} = -P_s\mathbf{n}$ but leads to the same conclusion: the boundary term $T_{\partial\Omega}$ vanishes if the test function φ is solenoidal and satisfies the same Dirichlet conditions than the velocity field, in particular $\varphi_{x_2} = \boldsymbol{\varphi} \cdot \mathbf{x}_2 = 0$ at the outlet. This is especially true if φ is a POD mode of a “fluctuant” velocity $\mathbf{u}^e - \bar{\mathbf{u}}^e$ where $\bar{\mathbf{u}}^e$ is a solenoidal field defined to satisfy the same Dirichlet boundary conditions than \mathbf{u}^e .

That explicit treatment of the boundary conditions is interesting if constructing such a solenoidal field $\bar{\mathbf{u}}^e$ which satisfies the Dirichlet boundary conditions is easy and cheap. This is especially true for unsteady Dirichlet conditions (a mean velocity field is suitable) or for Dirichlet conditions in the form

$$\bar{\mathbf{u}}^e(\mathbf{x}, t) = \mathbf{w}(\mathbf{x}, t) = \sum_{i=1}^K w_i(t) \boldsymbol{\psi}_i(\mathbf{x}) \quad \text{on } \Gamma_D, \quad (\text{A.9})$$

with K small: it suffices to solve K Stokes problems for each velocity profile $\boldsymbol{\psi}_i$. However, for complex unsteady Dirichlet boundary condition as in our step flow configuration, computing $\bar{\mathbf{u}}^e$ amounts to simulating the flow: the boundary term $t_{\partial\Omega}$ poses problems and must be neglected or modeled (or the velocity-vorticity formulation of Rempfer must be tested [22]). Fortunately, the inlet Dirichlet condition of our step flow is quasi-steady and $t_{\partial\Omega}$ can be neglected as first approximation since it takes small values at the inlet.

A.1. Important remark

Notice that the variational formulation (A.7) is available for a pseudo stress condition (A.3) but not for the stress condition $-\sigma\mathbf{n} = \boldsymbol{\beta}$ where

$$\sigma = \tilde{\sigma} + \frac{1}{Re} [\nabla u]^T = \frac{1}{Re} \left([\nabla u] + [\nabla u]^T \right) - pI_d \quad (\text{A.10})$$

is the physical stress tensor and now $\boldsymbol{\beta}$ the flow stress on Γ_N . That latter condition is used in particular in the work of Noack et al. [14] but is not considered in the variational formulation proposed.

However, that boundary condition could be explicitly taken into account in theory by keeping the zero divergence of ∇u^T in the incompressible expression of the Navier–Stokes equations. Indeed, the incompressible Navier–Stokes equations can be expressed for any $\omega \in \mathbb{R}$ as

$$\nabla \cdot \mathbf{u} = 0, \quad (\text{A.11})$$

$$\partial_t \mathbf{u} + (\mathbf{u} \cdot \nabla) \mathbf{u} - \nabla \cdot [(1 - \omega) \tilde{\sigma} + \omega \sigma] = \mathbf{h},$$

since $\nabla \cdot ([\nabla u]^T) = \nabla \cdot (\nabla \cdot \mathbf{u}) = 0$ (the case $\omega = 0$ corresponds to the classical expression of the incompressible Navier–Stokes equations). From the corresponding Navier–Stokes problem for $\omega = 1$ with Dirichlet conditions on Γ_D for the velocity and the condition (A.10) on $\Gamma_N = \partial\Omega \setminus \Gamma_D$, the following variational formulation is deduced for a solenoidal test function $\boldsymbol{\varphi}$ which satisfies homogeneous Dirichlet conditions on Γ_D :

$$\frac{d}{dt}(\mathbf{u}, \boldsymbol{\varphi}) + ((\mathbf{u} \cdot \nabla) \mathbf{u}, \boldsymbol{\varphi}) + \frac{1}{Re} \left(\sum_{i=1}^d (\nabla u_{x_i}, \nabla \varphi_{x_i}) + \sum_{i,j=1}^d (\partial_{x_i} u_{x_j}, \partial_{x_j} \varphi_{x_i}) \right) + \int_{\Gamma_N} \boldsymbol{\beta} \cdot \boldsymbol{\varphi} \, ds = (\mathbf{h}, \boldsymbol{\varphi}). \quad (\text{A.12})$$

In conclusion, it seems that the flux boundary condition (A.10) could be explicitly taken into account within a POD-Galerkin system as the pseudo stress condition. Such a system has not been constructed yet in the literature.

Appendix B. Case e affine

We suppose that e is an affine function of f , that is of its coefficients $y \in \mathbb{R}^P$ in the natural monomial basis $(m_k)_{1 \leq k \leq P}$ of the vector polynomials in M variables of degree 2 with M components (that natural basis is given for $M = 2$ in Appendix D). In the following, y^g and y^α will denote the coefficients of f^g (the original POD-Galerkin system) and f^α (the calibrated system), respectively; moreover $e(y, t) \equiv e(f, t)$, $\mathcal{E}(y) \equiv \mathcal{E}(f)$ and so on by notation abuse.

Hence, since e is affine,

$$e(\cdot, t) : \mathbb{R}^P \rightarrow \mathbb{R}^M, \quad y \mapsto E(t)y + e(0, t), \quad (\text{B.1})$$

where the columns of $E(t) \in \mathbb{R}^{M \times P}$ are the vectors $e(m_k, t) - e(0, t)$. Thus,

$$\langle \|e(f, t)\|_A^2 \rangle = \langle e(y, t)^T A e(y, t) \rangle = c - 2l^T y + y^T A y, \quad (\text{B.2})$$

with

$$c = \langle e(0, t)^T A e(0, t) \rangle, \quad (\text{B.3})$$

$$l = -\langle E(t)^T A e(0, t) \rangle \quad (\text{B.4})$$

and

$$A = \langle E(t)^T \Lambda E(t) \rangle. \quad (\text{B.5})$$

Since A is symmetric, the gradient of $(1 - \alpha)\mathcal{E}$ at y is $2\chi_A(Ay - l)$ with

$$\chi_A = \frac{(1 - \alpha)}{\left\langle \|e(f^g, t)\|_A^2 \right\rangle}. \quad (\text{B.6})$$

Therefore, if Π is the non-negative symmetric matrix associated to \mathcal{D} , the differential of \mathcal{J}^α is

$$\nabla \mathcal{J}^\alpha(y) : \mathbb{R}^P \rightarrow \mathbb{R}, \quad (\text{B.7})$$

$$\delta y \mapsto 2[(\chi_A A + \chi_\Pi \Pi)y - (\chi_A l + \chi_\Pi \Pi y^g)]^T \delta y,$$

where

$$\chi_\Pi = \frac{\alpha}{\|f^g\|_\Pi^2} \quad (\text{B.8})$$

and

$$\mathcal{J}^\alpha(y^\alpha) = \min_{y \in \mathbb{R}^P} \mathcal{J}^\alpha(y) \iff B^\alpha y^\alpha = l^\alpha, \quad (\text{B.9})$$

with

$$B^\alpha = \chi_A A + \chi_\Pi \Pi \quad \text{and} \quad l^\alpha = \chi_A l + \chi_\Pi \Pi y^g. \quad (\text{B.10})$$

If B^α is non-singular, the solution to the problem is unique and can be computed if this matrix is well conditioned.

Appendix C. Expressions of A and l for state and flow calibrations

With the notations of the preceding appendix, the expressions of A and l are with $\Lambda = I_M$

- for the state calibration ($e = e_2$):

$$A_{i,j} = \left\langle \left[\int_0^t m_i(a^e(\tau)) d\tau \right]^T \int_0^t m_j(a^e(\tau)) d\tau \right\rangle \quad (\text{C.1})$$

and

$$l_i = \left\langle \left[\int_0^t m_i(a^e(\tau)) d\tau \right]^T (a^e(t) - a^e(0)) \right\rangle \quad (\text{C.2})$$

- and for the flow calibration ($e = e_3$):

$$A_{i,j} = \left\langle m_i(a^e(t))^T m_j(a^e(t)) \right\rangle m \quad (\text{C.3})$$

and

$$l_i = \left\langle m_i(a^e(t))^T \dot{a}^e(t) \right\rangle. \quad (\text{C.4})$$

It is worth noting that, for $A = I_M$, A can be written in block diagonal form with identical blocks for both calibration methods (it depends on the order of the vector monomial basis). Therefore, if Π is block diagonal with identical blocks as well, the linear system $B^\alpha y^\alpha = l^\alpha$ can be split into M similar linear systems of dimension P/M ; in fact, any j th component f_j^α of f^α is solution to an minimization problem defined by α , the diagonal blocks $\tilde{\Pi}$ of Π , the vector $Y_{:,j}^g$ of coefficients of the j th component of f^g , a^e and \dot{a}_j^e : see below for more details in the case $M = 2$.

Appendix D. Linear systems obtained for $M = 2$

If $M = 2$, $P = 12$ and the natural vector monomial basis $(m_k)_{1 \leq k \leq P}$ is defined, for $a = (a_1 \ a_2)^T$ and for all $1 \leq i \leq P/M$, by

$$m_i(a) = \begin{pmatrix} \tilde{m}_i(a) \\ 0 \end{pmatrix}, \quad m_{i+(P/M)}(a) = m_{i+6}(a) = \begin{pmatrix} 0 \\ \tilde{m}_i(a) \end{pmatrix}, \quad (\text{D.1})$$

where $(\tilde{m}_k)_{1 \leq k \leq P/M}$ is the scalar monomial basis: $\tilde{m}_1(a) = 1$, $\tilde{m}_2(a) = a_1$, $\tilde{m}_3(a) = a_2$, $\tilde{m}_4(a) = a_1^2$, $\tilde{m}_5(a) = a_1 a_2$ and $\tilde{m}_6(a) = a_2^2$. Therefore, if $A = I_M$,

$$A = \begin{pmatrix} \tilde{A} & 0 \\ 0 & \tilde{A} \end{pmatrix} \quad \text{with } \tilde{A} \in \mathbb{R}^{(P/M) \times (P/M)} \quad (\text{D.2})$$

and

$$\tilde{A}_{i,j} = \begin{cases} \left\langle \int_0^t \tilde{m}_i(a^e(\tau)) d\tau \int_0^t \tilde{m}_j(a^e(\tau)) d\tau \right\rangle & \text{for } e = e_2, \\ \left\langle \tilde{m}_i(a^e(t)) \tilde{m}_j(a^e(t)) \right\rangle & \text{for } e = e_3. \end{cases} \quad (\text{D.3})$$

For instance,

$$\tilde{A}_{2,5} = \tilde{A}_{5,2} = \left\langle \int_0^t a_1^e(\tau) d\tau \int_0^t a_1^e(\tau) a_2^e(\tau) d\tau \right\rangle \quad \text{for } e = e_2 \quad (\text{D.4})$$

and

$$\tilde{A}_{2,3} = \tilde{A}_{3,2} = \tilde{A}_{1,5} = \tilde{A}_{5,1} = \left\langle a_1^e(t) a_2^e(t) \right\rangle \quad \text{for } e = e_3 \quad (\text{D.5})$$

($\tilde{A}_{2,3} \neq \tilde{A}_{1,5}$ for $e = e_2$). Thus, if Π is block diagonal with identical blocks as A is, the system $B^\alpha y^\alpha = l^\alpha$ of dimension $P = 12$ naturally divides into $M = 2$ similar systems of dimension $P/M = 6$ which can be written as a single linear system:

$$\tilde{B}^\alpha Y^\alpha = L^\alpha, \quad (\text{D.6})$$

where

- $\tilde{B}^\alpha = \chi_A \tilde{A} + \chi_\Pi \tilde{\Pi} \in \mathbb{R}^{(P/M) \times (P/M)}$ with $\Pi = \begin{pmatrix} \tilde{\Pi} & 0 \\ 0 & \tilde{\Pi} \end{pmatrix}$ (χ_A and χ_Π are defined in [Appendix B](#)),
- $Y^\alpha = (Y_{:,1}^\alpha \ Y_{:,2}^\alpha) \in \mathbb{R}^{(P/M) \times M}$ where the j th column $Y_{:,j}^\alpha$ of Y^α contains the coefficients of the scalar polynomial f_j^α in the monomial basis (\tilde{m}_k) (f_j^α is the j th component of f^α),
- $L^\alpha = \chi_A L + \chi_\Pi \tilde{\Pi} Y^g$ where $Y^g \in \mathbb{R}^{(P/M) \times M}$ contains the polynomial coefficients of the original POD-Galerkin system f^g as Y^α does for f^α and where $L \in \mathbb{R}^{(P/M) \times M}$ is defined by

$$L_{i,j} = \begin{cases} \left\langle \int_0^t \tilde{m}_i(a^e(\tau)) d\tau \quad (a_j^e(t) - a_j^e(0)) \right\rangle & \text{for } e = e_2 \\ \left\langle \tilde{m}_i(a^e(t)) \quad \dot{a}_j^e(t) \right\rangle & \text{for } e = e_3. \end{cases} \quad (\text{D.7})$$

For instance,

$$L_{6,1} = \left\langle \int_0^t a_2^e(\tau)^2 d\tau (a_1^e(t) - a_1^e(0)) \right\rangle \quad \text{for } e = e_2 \quad (\text{D.8})$$

and

$$L_{4,2} = \left\langle a_1^e(t)^2 \dot{a}_2^e(t) \right\rangle \quad \text{for } e = e_3. \quad (\text{D.9})$$

In fact, any solution $Y_{:,j}^\alpha$ to $\tilde{B}^\alpha Y_{:,j}^\alpha = L_{:,j}^\alpha$ corresponds to an optimal scalar polynomial f_j^α :

$$\mathcal{J}_j^\alpha(f_j^\alpha) \leq \mathcal{J}_j^\alpha(f) \quad (\text{D.10})$$

for all scalar polynomial f of degree 2 in M variables with

$$\mathcal{J}_j^\alpha(f) = \chi_A \Lambda_{j,j} \mathcal{E}^j(f) + \chi_\Pi \mathcal{D}^j(f), \quad (\text{D.11})$$

where

$$\mathcal{E}^j(f) = \begin{cases} \left\langle \left[a_j^e(t) - a_j^e(0) - \int_0^t f(a^e(\tau)) d\tau \right]^2 \right\rangle & \text{for } e = e_2, \\ \left\langle \left[\dot{a}_j^e(t) - f(a^e(t)) \right]^2 \right\rangle & \text{for } e = e_3, \end{cases} \quad (\text{D.12})$$

$$\mathcal{D}^j(f) = \|f - f_j^g\|_{\Pi}^2 = (y - Y_{:,j}^g)^T \tilde{\Pi} (y - Y_{:,j}^g) \quad (\text{D.13})$$

if $y \in \mathbb{R}^{P/M}$ is the vector of the polynomial coefficients of f in the scalar monomial basis $(\tilde{m}_k)_{1 \leq k \leq P/M}$.

References

- [1] P. Holmes, J. Lumley, G. Berkooz, Turbulence, Coherent Structures, Dynamical Systems and Symmetry, Cambridge University Press, Cambridge, MA, 1998.
- [2] S. Ravindran, A reduced-order approach for optimal control of fluids using proper orthogonal decomposition, *Int. J. Numer. Meth. Fluids* 34 (2000) 425–448.
- [3] S. Ravindran, Reduced-order adaptive controllers for fluid flows using POD, *J. Sci. Comput.* 15 (4) (2000) 457–478.
- [4] M. Fahl, Trust-region methods for flow control based on reduced order modelling, Ph.D. thesis, Universität Trier (2000).
- [5] A. Iollo, S. Lanteri, J. Désidéri, Stability properties of POD-Galerkin approximations for the compressible Navier-Stokes equations, *Theoret. Comput. Fluid Dynamics* 13 (2000) 377–396.
- [6] N. Aubry, P. Holmes, J. Lumley, E. Stone, The dynamics of coherent structures in the wall region of a turbulent boundary layer, *J. Fluid Mech.* 192 (1988) 115–173.
- [7] B. Podvin, On the adequacy of the ten-dimensional model for the wall layer, *Phys. Fluids* 13 (2001) 210–224.
- [8] M. Couplet, P. Sagaut, C. Basdevant, Intermodal energy transfers in a proper orthogonal decomposition-Galerkin representation of a turbulent separated flow, *J. Fluid Mech.* 491 (2003) 275–284.
- [9] S. Sirisup, G. Karniadakis, A spectral viscosity method for correcting the long-term behavior of POD models, *J. Computat. Phys.* 194 (2004) 92–116.
- [10] B. Galletti, C. Bruneau, L. Zannetti, A. Iollo, Low-order modelling of laminar flow regimes past a confined square cylinder, *J. Fluid Mech.* 503 (2004) 161–170.
- [11] G. Vigo, Méthodes de décomposition orthogonale aux valeurs propres appliquées aux écoulements instationnaires compressibles complexes, Ph.D. thesis, Paris IX Dauphine (2000).

- [12] I. Mary, P. Sagaut, M. Deville, An algorithm for unsteady viscous flows at all speeds, *Int. J. Numer. Meth. Fluids* 34 (2000) 371–401.
- [13] L. Sirovich, Turbulence and the dynamics of coherent structures, *Quart. Appl. Math.* XLV (3) (1987) 561–590.
- [14] B. Noack, K. Afanasiev, M. Morzynski, G. Tadmor, F. Thiele, A hierarchy of low-dimensional models for the transient and post-transient cylinder wake, *J. Fluid Mech.* 497 (2003) 335–363.
- [15] O. Labb  , P. Sagaut, E. Montreuil, Large-Eddy Simulation of heat transfer over a backward-facing step, *J. Numer. Heat Transfer A* 42 (2002) 73–90.
- [16] W. J  rgens, H.-J. Kaltenbach, Eigenmode decomposition of turbulent velocity fields behind a swept, backward-facing step, *J. Turbulence* 4 (018) (2003).
- [17] O. R  ssler, An equation for continuous chaos, *Phys. Lett. A* 57 (5) (1976) 397–398.
- [18] E. Lorenz, Deterministic nonperiodic flow, *J. Atmos. Sci.* 20 (2) (1963) 130–148.
- [19] C. Foias, I. Kukavica, M. Jolly, E. Titi, The Lorenz equations as a metaphor for the Navier–Stokes equations, *Discrete Continuous Dynamical Syst.* 7 (2) (2001) 403–429.
- [20] D. Rempfer, H. Fasel, Dynamics of three-dimensional coherent structures in a flat-plate boundary layer, *J. Fluid Mech.* 275 (1994) 257–283.
- [21] R. Sani, P. Gresho, Resume and remarks on the open boundary condition mini-symposium, *Int. J. Numer. Meth. Fluids* 18 (1994) 983–1008.
- [22] D. Rempfer, Investigations of boundary-layer transition via galerkin projections on empirical eigenfunctions, *Phys. Fluids* 8 (1996) 175–188.